Official English translation

Nonlinear dynamical models of neurons: Review

A. S. Dmitrichev, D. V. Kasatkin, V. V. Klinshov, S. Yu. Kirillov,
O. V. Maslennikov, D. S. Shchapin, V. I. Nekorkin

Institute of Applied Physics of RAS
46, Ul'yanov st., 603950 Nizhny Novgorod, Russia
E-mail: admitry@neuron.appl.sci-nnov.ru, kasatkin@appl.sci-nnov.ru, vladimir.klinshov@gmail.com,
skirillov@ipfran.ru, olmaov@ipfran.ru, shapinds@mail.ru, vnekorkin@neuron.appl.sci-nnov.ru
Received 01.06.2018, accepted for publication 28.06.2018

Topic. A review of the basic dynamical models of neural activity is presented and individual features of their behavior are discussed, which can be used as a basis for the subsequent development and construction of various configurations of neural networks. The work contains both new original results and generalization of already known ones published earlier in different journals. **Aim** is to familiarize the reader with the basic dynamical properties of neurons, such as the existence of a rest state and the generation of the action potential; to outline the dynamical mechanisms underlying these properties which are used in the development of neural models with various levels of detailing. **Investigated models.** From the mathematical point of view, neuron models are divided into two classes. The first class is represented by models with continuous time described by ordinary differential equations. The section devoted to continuous-time models starts from the most detailed Hodgkin–Huxley model, which is a canonical model for neural activity in nonlinear dynamics. Further we describe simplified models, such as a two-dimensional model of Morris–Lecar for spiking and a three-dimensional model of Hindmarsh–Rose for bursting. The FitzHugh–Nagumo model is described in detail, and detailed bifurcation analysis is presented. We also present models for neurons with specific properties, namely a neuron with afterdepolarization and an inferior olives neuron. The last and the simplest model is the «integrate–fire» model. The second class of neural models are systems with discrete time represented by discrete maps. Such models have recently gained increasing popularity due to the richness of the demonstrated dynamics and the ease of numerical simulations. We describe such models as the Chialvo model, the Izhikevich model, the Rulkov model, and the Courbage–Nekorkin model. **Results.** The basic physical principles underlying the construction of mathematical models of neural activity, based on ion transport, are outlined. Using the FitzHugh–Nagumo model as an example, the main properties and mechanisms of the emergence of multithreshold excitation regimes in neurons are described. The mechanism of formation of burst oscillations in the Hindmarsh–Rose model is outlined. A dynamic mechanism for temporal decline of the excitation threshold and the emergence of periodic oscillations in a neuron with afterdepolarization are described. The formation of (Ca2+)- and (Na2+)-dependent spikes in inferior olive neurons is described. Dynamic mechanisms of formation of the major regular and chaotic regimes of neural activity in discrete models of Chialvo, Izhikevich, Rulkov and Courbage–Nekorkin are described. **Discussion.** In the Conclusion we briefly summarize the content of the survey.

Keywords: dynamical systems, neurons, bifurcations.

https://doi.org/10.18500/0869-6632-2018-26-4-5-58

Reference: Dmitrichev A.S., Kasatkin D.V., Klinshov V.V., Kirillov S.Yu., Maslennikov O.V., Shchapin D.S., Nekorkin V.I. Nonlinear dynamical models of neurons. *Izvestiya VUZ, Applied Nonlinear Dynamics,* 2018, vol. 26, iss. 4, pp. 5–58. https://doi.org/ 10.18500/0869-6632-2018-26-4-5-58

Introduction

Neurons (or nerve cells) are basic structural and functional units of nervous system. A neuron, like any other biological cell, represents a cell body of about 10–100 μm covered by a membrane. This membrane is an impenetrable double layer of lipids. The distinctive feature of neural membrane is the presence of the electric potential difference between the inner and the outer surfaces. This difference, which is called the membrane potential, has a certain constant negative value at rest and can vary with time. The electrical pulses generated by the membrane code and transfer the information in neural networks. The transmission of electrical signals among neurons takes place as a result of the propagation of these signals through special cell processes spreading from the cell body in the form of thin tubular fibers. The two types of these processes are axons and dendrites. An axon is a long process that transmits electrical signals from the neuron body to other cells. Dendrites are usually shorter branching processes along which impulses received from other cells are transmitted to neuron. Axons have numerous terminal fibers at their ends. These fibers can contact with dendrites, axons or other cell bodies. The contact takes place via special structures called synapses (see Fig. 1). The synapse consists of two membranes (presynaptic and postsynaptic) of contacting neurons. The chemical and the electrical synapses are the main types. The distance between the membranes of presynaptic and postsynaptic neurons in the electrical synapse is about 2–4 nm and their interaction is carried out with the help of special proteins. The contact between neurons in the chemical synapse is completely different. In this case the membranes of the interacting neurons are situated at the distance of about 20–40 nm from each other and form a synaptic cleft. When an electric signal reaches the presynaptic terminal its membrane releases a substance called a neuromediator. The neuromediator enters the synaptic cleft, passes through it and affects the receptor of the postsynaptic membrane, changing its potential, and therefore is responsible for the connection between neurons. Synapses are different both in the type of the neuromediator and in their functional properties. If the membrane potential of the postsynaptic neuron gets close to the cut off under the influence of neuro-

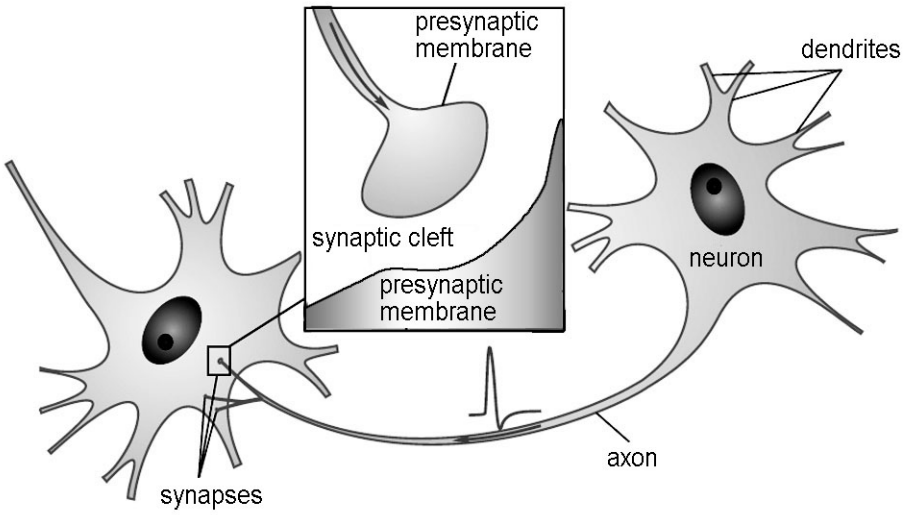

Fig. 1. Schematic representation of a neuron and a synapse

mediator, i.e. depolarization of the membrane takes place, the synapse is called excitatory. Otherwise, if the membrane potential of the postsynaptic neuron is farther from the cut off and hyperpolarization of the membrane takes place, the synapse is called inhibitory or suppressive.

The basic form of neuronal electrical activity is so-called action potential, i.e. an electrical pulse or a spike. Being unexcited the neural membrane is polarized and its inner surface has a negative potential against the outer one. This resting potential is usually about (-70)–(-90) mV. When the action potential occurs one can observe the rising edge. At that time the membrane potential grows rapidly to the peak value of $(+20)$–$(+40)$ mV and the excitation peak is observed for some time. Then the repolarization phase takes place. During the phase the membrane potential decreases to the meaning lower than the initial one. The total duration of the action potential in nerve cells is about 1 ms, after which residual effects in the membrane can be observed for 1–3 ms. It is a period of adiaphoria during which the membrane is unexcitable. The characteristics of action potentials are practically identical in all nerve cells of the organism. They are universal data storage carriers in neural networks.

The action potential occurs under the influence of different stimuli such as depolarization, i.e. changing of the membrane potential into a positive one. The appearance of the action potential follows the law of all or nothing. This means that there is an excitation threshold and when the stimulus is too weak (it does not exceed the threshold) the cell membrane does not respond; on the contrary, when the stimulus is strong (it exceeds the threshold) the membrane responds with the pulse of fixed amplitude, which does not depend on the stimulus amplitude.

Besides induced generation of action potentials in different nerve cells one can observe other forms of electrical activity. For instance, in some cells the generation of electric pulses occurs spontaneously without external excitation. These are called pacemakers. They represent the cells which set the rhythm and form the rhythmic activity of neural networks. External stimulation of such cells can lead to rhythm tuning and the change of the amplitude or the frequency of generated pulses. Spontaneous or induced generation of bursts i.e. packs of pulses, is another widely-spread type of electrical activity. In this case periods of pulse generation alter with slack periods. Both regular and chaotic generations of bursts are observed. Neural bursting plays an important role in data transfer process, generation and synchronization of rhythms in neural networks.

The above listed types of neural activity refer to excited states of neuron. But often membrane potential dynamics lower than the threshold of excitation is of importance. For instance, one can see spontaneous subthreshold oscillations of membrane potential in some types of neurons. While stimulating such neurons, spikes of different amplitude may appear in peaks of subthreshold oscillations. Moreover, excitability of nerve cells can also change due to subthreshold dynamics of membrane potential. For example, membrane potential can have temporary deviations from the equilibrium value after the generation of action potential. Such deviations can be both positive (postdepolarization) and negative (posthyperpolarization). In the first case the following excitation of neuron is facilitated, while in the second case it is obstructed.

The history of neural activity simulation is long. Current neuron models which we encounter in neuroscience can be divided in two classes. The first one is formed by the formal or neuron-like elements, while the second class includes the models in the form of nonlinear dynamical systems.

The concept of the formal neuron was firstly suggested in the article by McCulloch and Pitts [1]. Formal neurons are threshold elements performing input-output conversion. At the input such neuron gets a stimulus vector which is previously multiplied by the weight vector. The weight indices simulate the action of synapses. Then the coordinates of the stimulus vector are summed up and the resulting sum undergoes nonlinear transformation. Consequently the output of the formal neuron has a signal that can be both a scalar variable and a vector. Further, this signal is sent to the inputs of other neurons thus forming up an artificial neural network. At present these networks are widely used for solving problems in science and engineering. However, from neurophysiological point of view, in order to simulate the processes of brain activity, which occur while performing cognitive functions, a more relevant neuron model is required. We will get such models if we take into account the fact that neurons have ion channels due to which ion currents appear and the change of membrane potential takes place. Since these processes are evolutionary corresponding mathematical models have the form of nonlinear dynamical systems. In present survey we take into consideration the neuron models of this class and begin with the classical Hodgkin–Huxley model.

The article consists of two parts. The first part describes physical principles which form the basis of nerve cell excitability. The second part is devoted to the continuous time models. This part presents basic information about the Hodgkin–Huxley model. Further we describe the models of Morris–Lecar, FitzHugh–Nagumo, Hindmarsh–Rose, the neuron model with aferdepolarization, the inferior olives neuron model and the integrate-and-fire model. The second part also presents the ways of describing neurondynamics applying discrete time systems. We examined different modes of neural activity which are simulated in the Chialvo model, the Izhikevich model, the Rulkov model and the Curbash–Nekorkin model. In conclusion we briefly state mathematical aspects presented in the survey.

1. Physics of Neural Excitability

Physicochemical basis of nerve cell excitation includes the processes of ion transport through cell membrane. Four types of ions are engaged in this process. They are K^+, Na^+, Ca^{2+}, Cl^-. Although the membrane is a lipid bilayer, which is impenetrable for these ions, it has specific protein systems, which are embedded in it. They provide ion transport through cell membrane. There are two types of such systems: ion pumps and ion channels. The ion pump consists of integral proteins which provide active ion transport against the concentration gradient. As a result of the work done by ion pumps transmembrane ion gradients are created and maintained as the concentration of sodium, calcium and chlorine is lower inside than outside the cell (in the intercellular fluid), while the concentration of potassium is higher inside the cell. The difference of ion concentration inside and outside the cell leads to non-zero reversal potential appearance for the given type of neurons and consequently distinct from zero membrane potential.

Ion channels are integral proteins providing passive ion transport along the electrochemical gradient. There are nonselective channels which transmit all the types of ions and are constantly conductive, and selective ones which transmit only a certain type of ions. There are special types of channels for every type of ions. These channels can change their conductance, the can open and close. Changes in the condition of selective

channel depend on the so called gates. These are special protein molecules which change their conformation in response to the signals of different types.

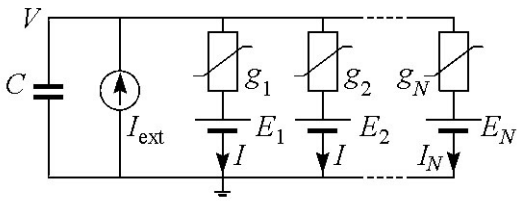

Fig. 2. Electronic equivalent circuit for a neural membrane

According to the type of signal which causes opening and closing of the selective gates they can be divided into several basic classes. Potential-depending and chemosensitive ion channels are the most important classes. The condition of the first ones depends on the value of transmembrane potential. The channels of this class play an important role in the processes of action potential generation. The condition of the channels from the second class changes after attaching of ligand molecules, e.g. neurotransmitter, to the channel-associated receptor protein. The channels of this class play an essential role in the processes of chemical synaptic transmission. There are also selective channels. Their properties alter under the influence of mechanical power, light and changes of temperature or pressure. These channels are of utmost importance in the processes of obtaining sensory information, e.g. in sensory neurons.

The capacity of cell membrane to store the charge on its inner surface allows us to consider it an electric condenser with certain capacitance. Ion currents, flowing through the membrane, charge or discharge this condenser. Therefore, neuron can be represented as electronic equivalent circuit shown in Fig. 2. Applying Kirchhoff's equation for the currents which pass through the surface of the cell membrane we get the following equation:

$$C\frac{dV}{dt} = I_{ext} - \sum_{j=1}^{N} I_j, \tag{1}$$

Where V is electrical potential of cell membrane, C is membrane capacitance, I_{ext} is external current and I_j stands for ion currents flowing through the channels of different types. The intensity of each ion current is defined by reversal potential E_j for the corresponding ion type and by conductance of corresponding channels g_j:

$$I_j = g_j(V - E_j). \tag{2}$$

The equations (1)–(2) are the basic equations of transmembrane ion transport. There is a big class of neuron models based on these equations. These models differ in quantity, in the type of relevant ion channels and the ways of describing selective channels conductance, which changes dynamically with the time due to opening and closing of the channels.

2. Neural Activity Models with Continuous Time

2.1. The Hodgkin – Huxley Model. The first historically known model based on ion transport is the model offered by English neurophysiologists Hodgkin and Huxley [2]. They carried out their experiments on a squid gigantic axon and studied the mechanisms of nervous excitement appearance and its transmission. Hodgkin and Huxley described

that selective channel conductance is defined by the condition of so called activation and inactivation gates. The activation gates open gradually when the membrane potential rises while the inactivation gates close. The conductance of j-type channels is defined by the following expression:

$$g_j = \overline{g}_j a_j^{p_j} b_j^{q_j}, \tag{3}$$

Where $\overline{g}_j$ is the maximum conductance of channels in the open state, a_j and b_j are activation and inactivation variables respectively, which characterize the probability of being in the open state of activation and inactivation gates respectively, and p_j and q_j are positive integers which define the number of activation and inactivation gates per ion channel. Hodgkin and Huxley suggested that dynamics of activation and inactivation variables is described with the help of differential equations of the first order.

$$\frac{dx}{dt} = \frac{x_\infty(V) - x}{\tau_\infty(V)}. \tag{4}$$

where $x = a_j$, b_j is the vector of variables, $x_\infty(V)$ and $\tau_\infty(V)$ define the steady-state conditions of the variables and the relaxation time of the processes which generally depend on the membrane potential value. Hodgkin and Huxley discovered that sodium and potassium ions play the main role in ion transport. It is the model they suggested that describes sodium and potassium channels in detail. Hodgkin and Huxley showed experimentally that sodium channels have one inactivation and three activation gates ($p_{Na} = 3$, $q_{Na} = 1$), while potassium ones have four activation gates per channel ($p_K = 4$, $q_K = 0$). These numbers were chosen empirically so that to describe current kinetics in a better way. The functions $x_\infty(V)$ and $\tau_\infty(V)$ were also chosen empirically. Finally, the Hodgkin–Huxley model appears as follows:

$$C\frac{dV}{dt} = I_{ext} - \overline{g}_K n^4 (V - V_K) - \overline{g}_{Na} m^3 h (V - V_{Na}) - \overline{g}_L (V - V_L), \tag{5}$$

$$\frac{dx}{dt} = \alpha_x(V)(1 - x) - \beta_x(V)x. \tag{6}$$

Here V stands for membrane potential which is measured out in millivolts beginning with resting potential, $x = n, m, h$, where n and m are activation variables for potassium and sodium channels respectively and h is an the inactivation variable of sodium channels.

In case the biological parameters are relevant, tabular integration of the system (5)–(6) shows that this model simulates dynamics of neuron membrane potential in a proper way. The main property of the system is the action potential generation which follows the all-or-nothing law. Fig. 3 compares the graphs which show membrane potential dynamics of the squid gigantic axon and the Hodgkin–Huxley model. It is evident that the pulse shape produced by the model is close to the experimentally available shape of the waves and action potential is followed by the refractority phase. Not only qualitative but

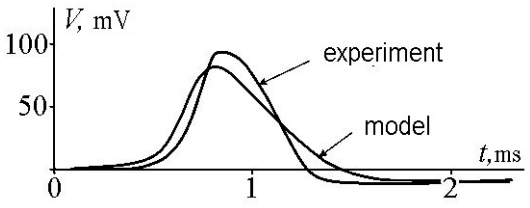

Fig. 3. Comparison of the action potential experimentally observed in the giant squid axon and the results of numerical integration of the Hodgkin–Huxley model. Modified from [2]

quantitative similarity of model dynamics and real membrane behavior are observed. The duration and the amplitude of the pulses shown in Fig. 3 match with a good degree of accuracy.

The principles which form the basis of the Hodgkin–Huxley model were used by other researchers to create similar models (see [3, 5]). These models differ in quality and the type of the ion channels taken into consideration. The main advantage of the Hodgkin–Huxley model is the detailed description of ion channels dynamics, biological adequacy and matching of the model and physiological parameters. However the complexity of analytical and numerical research caused the necessity of using simpler models of neural activity.

2.2. The Morris–Lecar Model. Another well-known model based on the Hodgkin–Huxley model was suggested by C. Morris and G. Lecar [6] to describe different modes of oscillatory activity which was observed during the experiments on giant barnacle muscle fiber. Experimental data [7] were used to make a 3-dimensional model which took into account two potential-dependent calcium and potassium ion channels which are never fully inactivated. The work [6] presents the analysis of possible modes, which are predicted by the theoretical model, and comparison with experimental data. Analyzing the modes, which satisfied oscillatory behavior of muscle fiber potential, it was suggested that calcium and potassium channel conductance has different relaxation time. Due to this the reduced model of the second order was obtained, taking into account that calcium channel conductance takes the stationary value immediately:

$$C\frac{dV}{dt} = I_{ext} - g_L(V - V_L) - g_{Ca}M_\infty(V)(V - V_{Ca}) - g_K n(V - V_K), \quad (7)$$

$$\frac{dn}{dt} = \frac{n_\infty(V) - n}{\tau_n(V)}.$$

The variables V and n are of the same meaning as in the Hodgkin–Huxley model. The summands in the right-hand side of the equation (7) determine the external current, the leakage current, and calcium and potassium currents flowing through the membrane. The functions $M_\infty(V)$, $n_\infty(V)$ and $\tau_n(V)$ are written as following:

$$M_\infty(V) = 0.5\left[1 + \tanh\left(\frac{V - V_1}{V_2}\right)\right],$$

$$n_\infty(V) = 0.5\left[1 + \tanh\left(\frac{V - V_3}{V_4}\right)\right],$$

$$\tau_n(V) = \left[\phi\cosh\left(\frac{V - V_3}{2V_4}\right)\right]^{-1}.$$

With the help of this simplified model it became possible to describe the series of oscillatory regimes (underdamping and periodic oscillations) fixed during the experiments on barnacle muscle fiber. Because of its relative simplicity the Morris–Lecar model (M–L) is one of the popular models built on the basis of the equations for ion transport This model is used for oscillatory activity simulation including nerve tissue.

Dynamics of the model (7) was examined in some papers [8–12]. These papers were focused mostly on the study of the external current influence on the nature of oscillation

appearance. The study of the bifurcation structure of the Morris–Lecar model in the planes with different parameters is given in [11] in detail. Due to the analysis of two-parameter bifurcation diagrams performed in this paper, where the external current I_{ext} and one the values g_{Ca}, ϕ, V_3 or V_4 were chosen as control parameters, it was possible to mark the regions with different behavior of membrane potential and find the ways which led to setting of these modes. System (7) can perform the regime of periodic pulse generation and the excitable regimes of different complexity. In general, the system behavior is specified by the number of attractors, mutual arrangement of saddle separatrixes and unstable limit cycles, existing in phase plane with the chosen parameter values. There are two types of attractors in the M–L model. They are the stable states of equilibrium and the limit cycles which respond to the resting state and periodic pulse generation of neuron when neural activity is described. Depending on the parameters dynamics of the M–L model can be monostable, bistable and even tristable. It is determined that the system (7) can have from one up to three equilibrium states, which is defined by the number of cross points of the system nullclines (see Fig. 4). When the system has three states of equilibrium one of them (O_2) is the saddle. Its stable separatrixes set the threshold of neuron excitation. The simplest example of the excitable regime is shown in Fig. 4, *a*). At the start time the system is in the resting state which is characterized by the stable equilibrium O_1 on the phase plane and which is the only one system attractor. The representative point is in the equilibrium state. The shift of this point takes place on the phase plane under the external stimulus. When the stimulus is over, the system returns to the resting state. If the stimulus is strong enough the response is characterized by the prominent growing change of the variable V, i.e. the system generates the excitation pulse. The system (7) can demonstrate a more complex excitable behavior when the generation of the series of excitation pulses is observed in response to the external stimulus (Fig. 4, *b*). Such behavior is fixed when the system parameters are close to bifurcation values which respond to the appearance of the double limit cycle. The appearance of the complex response is stipulated by the formation of "layering" on the phase plane. This formation is connected with the condensation of phase trajectories. The condensation, in turn, is the result of the system dynamic memory about the recent presence of the double limit cycle. When the system trajectory enters one of such "layerings", while returning to the state of equilibrium O_1, it makes a number of revolutions, which means the generation of the series of excitation pulses.

The regime of the periodic generation of excitation pulses is determined by the appearance of the stable limit cycle on the phase plane of the system (see Fig. 4, *c, d*). The regime of periodic oscillations can appear as a result of different bifurcations such as [11] Andronov–Hopf bifurcation, bifurcation of double limit cycle and the one of the loop of saddle-node separatrices.

The system (7) can demonstrate bistable behavior having excitable and oscillatory properties at the same time. The example of the phase portrait corresponding to such behavior is presented in the Fig. 4, *e*. There are a couple of limit cycles on the phase plane which are stable and unstable, and three equilibrium states one of which (O_1) is stable. If under the stimulus the representative point remains inside the region limited by the unstable limit cycle and happens to appear lower than stable separatrices of the saddle (O_2), the system generates the excitation pulse (Fig. 4, *e*). If after the influence of stimulus parameters the representative point on the phase plane turns out to be outside the region given off by the unstable limit cycle, the system switches to the regime of periodic oscillations corresponding to the stable limit cycle.

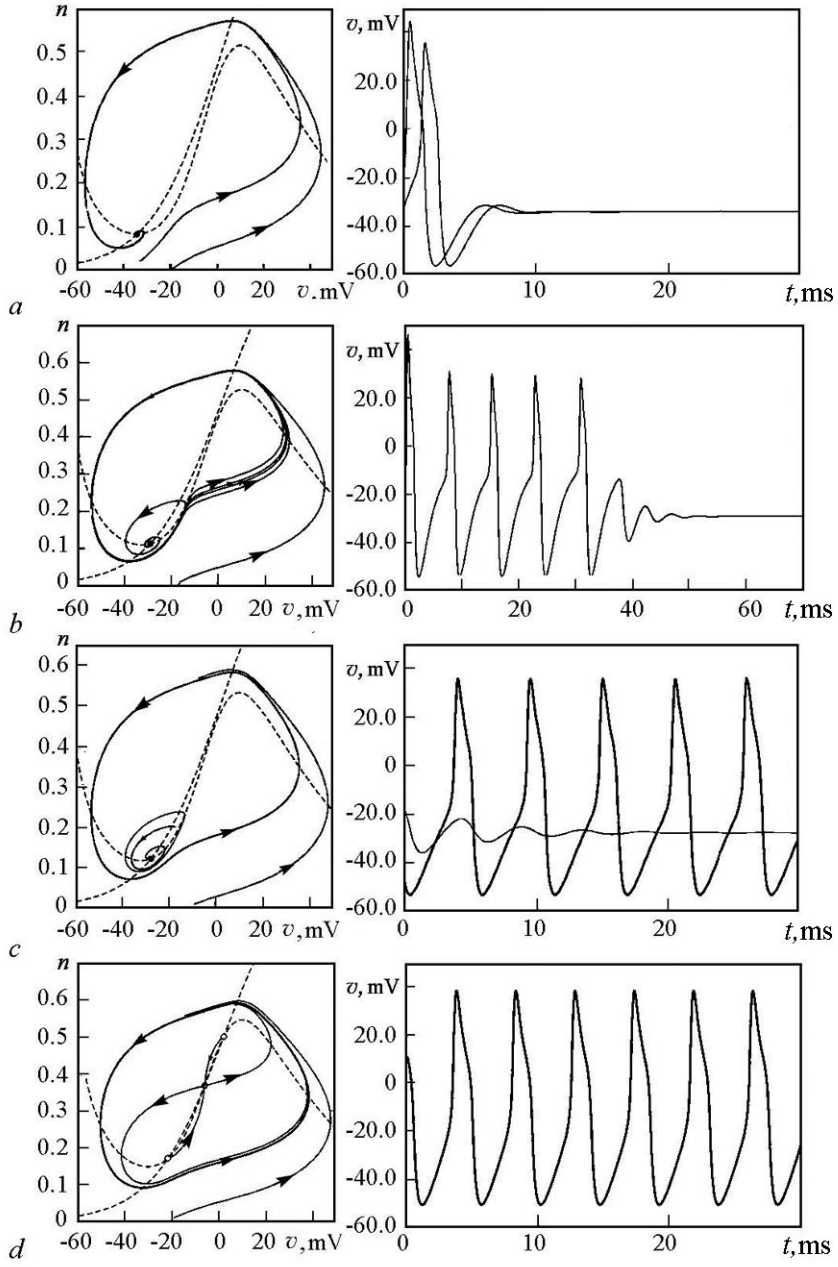

Fig. 4. Phase portraits and waveform of membrane potential in Morris–Lecar model for $C = 20$ μF/cm^2, $g_L = 0.2$ mS/cm^2, $g_{Ca} = 4.4$ mS/cm^2, $g_K = 8.0$ mS/cm^2, $V_l = 50$ mV, $V_{Ca} = 100$ mV, $V_K = 70$ mV, $V_1 = -1$ mV, $V_2 = 15$ mV, $V_3 = 2$ mV, $V_4 = 30$ mV, $\phi = 0.05$ s^{-1} and for different value of external current I_{ext} μA/cm^2: *a* – 20, *b* – 27.54842, *c* –30, *d* – 40

Finally, there are parameter regions where the system has three attractors [11]. They are two equilibrium states and a limit cycle. In this case the external stimulation causes generation of excitation pulses which ends up by returning to the resting state or it is possible to switch the system to the regime of periodic oscilations.

2.3. The FitzHugh–Nagumo Model. It was mentioned above that dynamics of the selective ion channel is characterized by some properties. Firstly, when the transmembrane potential V is fixed the current value I is set constant $I_\infty(V)$. Secondly, this value does not set instantly but during some period of time $\tau(V)$. Without elaborating on dynamics of ion channels we can use an ordinary linear differential equation to simulate these properties (see [13]):

$$\frac{dI}{dt} = \frac{I_\infty(V) - I}{\tau(V)}. \tag{8}$$

FitzHugh was the first to use the model with a simplified way of describing dynamics of nerve cell ion channels [14, 15]. Then it was extended by Nagumo with the example of spatially-extended systems [16]. The FitzHugh–Nagumo model uses the approach based on dividing the currents according to their time scales (see [17]). It is supposed that periods of time for current setting are small for most ion channels. Due to that it is possible to take the total current passing through them I_Σ as always equal to its equilibrium value $f(V)$. There is also one or some types of channels I, where the time of current change $\max_V \tau(V)$ is comparable and considered to be long. The equation (8) is used to describe these currents. The equation (5) describes dynamics of transmembrane potential. As a result, we get the following generalized two-dimensional FitzHugh–Nagumo system:

$$\begin{cases} \dot{V} = I_{ext} - I - f(V), \\ \dot{I} = \varepsilon(g(V) - I), \end{cases} \tag{9}$$

where $\varepsilon = C/\max\tau(V)$. Using the functions f and g from the original paper by FitzHugh and having changed the variables we get the classical FitzHugh–Nagumo system:

$$\begin{cases} \dot{u} = u - u^3/3 - v + I_{ext}, \\ \dot{v} = \varepsilon(u - a - bv). \end{cases} \tag{10}$$

where u describes dynamics of neuron membrane potential and v is the collective effect of all slow ion currents responsible for the restoration of the membrane resting potential. The a and b parameters provide conductance characteristics of ion channels and ε ($\varepsilon > 0$) means the rate of slow ion current changing.

Initially, the b and ε parameters had the following conditions: $0 < b < 1$, $\varepsilon \ll 1/b$. The first condition lets the system (10) have only one equilibrium state corresponding to the neuron resting state. The second condition, on the one hand, provides the opportunity of stability equilibrium changing into this state and, on the other hand, it lets system dynamics become close to the relaxation one. Therefore, regardless of the system parameters, its dynamics is formed by the so called fast and slow motions [18–21]. The first ones occur along the curve $v \approx \mathrm{const}$. The second ones occur in the ε-region of the stable manifold of slow motions, which is formed by the two dropping sections of u-nullcline ($v = u - u^3/3 + I_{ext}$). The left dropping section (in the region of the negative membrane potential) is usually associated with the refractory (or unexcited) state of neuron and

the right dropping section (in the region of the positive membrane potential) is associated with the excited state.

Let us take a closer look at typical regimes of the classical FitzHugh–Nagumo system. Their phase portraits are shown in Fig. 5, *a–f*. Fig. 5, *g–i* show the responses of the system in these regimes. The regime in Fig. 5, *a* is actual when $a > a^+$. The equilibrium state *O* is globally stable in this regime and located in the left region of the stable manifold of slow motions. Thus stimulus can make the system generate single excitation pulses (action potential or spikes). That is why this regime is called excitable. Actually, if the stimulus is strong enough, the representative point (C_0 trajectory) can leave the region the equilibrium state and get over threshold manifold which is formed by the layer of unstable slow motions occurring in the ε-region of the rising section of u-nullcline and its trace in the reverse time (the region is marked with grey in Fig. 5, *a*). Then following fast motions the representative point goes to the right section of the stable manifold of slow motions, moves along it to the discontinuity point, and then, following fast motions again, returns to the left region relaxing to the steady state in the end. When $a = a^+$ the Andronov–Hopf bifurcation and the change of equilibrium state stability take place. When $a < a^+$ decreases, a small limit cycle (C_1. See Fig. 5, *b*) appears on the phase plane of a neuron. This cycle responds to the quasiharmonic subthreshold oscillations. Then the system goes through a cascade of so called duck solutions [20]. The latter contain both the regions of the variety of fast and stable slow motions, and the regions of unstable

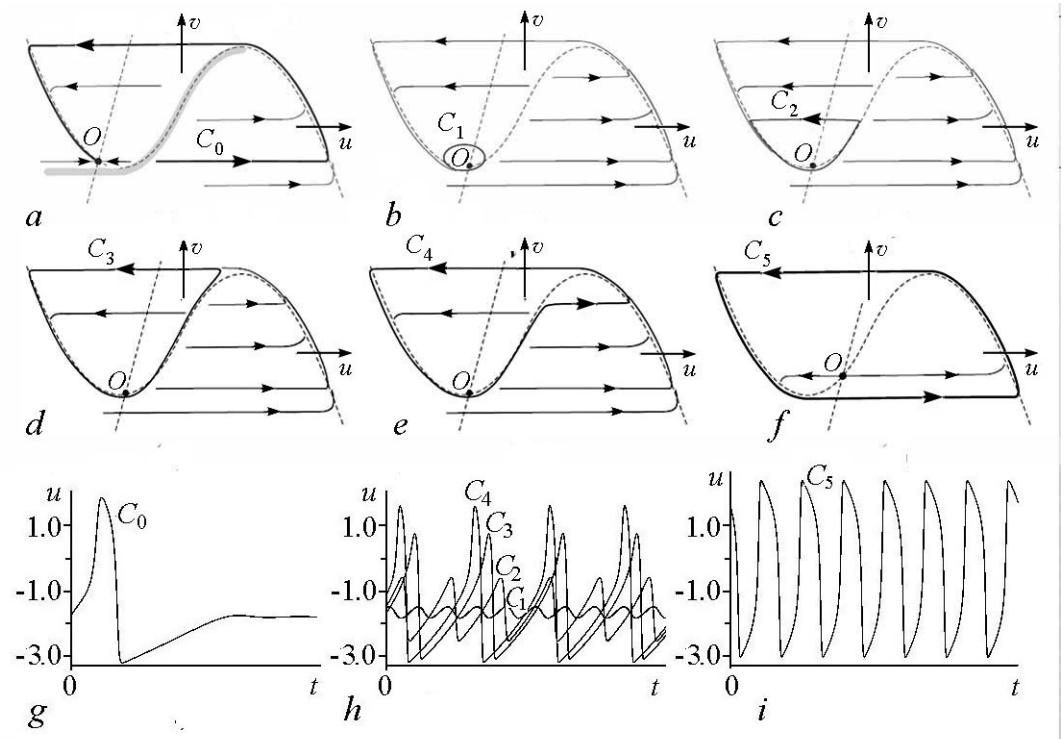

Fig. 5. Typical regimes of classical FitzHugh–Nagumo system: (*a*, *e*, *f*) – regimes of single and periodic generation of excitation pulses (action potentials or spikes); (*b–d*) – regimes of subthreshold oscillations; (*g–i*) – typical responses in the regimes. The dashed lines represent the system's nullclines. The parameters: (*a*) – $a > a^+$; (*b–f*) – $a \in (a^-, a^+)$, $a^{\mp}(\varepsilon, b, I_{ext}) = u_{1,2} - b(u_{1,2} - u_{1,2}^3/3 + I_{ext})$, $u_{1,2} = \mp\sqrt{1 - b\varepsilon}$

slow motions. These solutions respond to complex subthreshold (Fig. 5, *c, d*) and spike (Fig. 5, *e*) oscillations of the system. At first, the small limit cycle changes into the so called "headless duck" (C_2). This solution is called so, because it contains only one left region of stable manifold of slow motions. Then the small duck turns into a big "headless duck" (C_3) and that one becomes the duck with the head (C_4). The latter contains both the left and the right regions of stable manifold of slow motions. Finally, the big duck with the head changes into the big limit cycle (C_5. See Fig. 5, *f*). The neuron, in turn, switches to the regime of the periodic generation of excitation pulses. When a decreases further we can observe the reverse cascade of duck solutions, when $a = a^-$ the Andronov–Hopf bifurcation takes place and the equilibrium state becomes stable again, going to the right region of stable manifold of slow motions. The excitable regime arises in the system.

At present the classical FitzHugh–Nagumo system is widely applied in different areas of modern science. However, it is difficult to apply this system to describe neuron dynamics because of certain properties. Threshold manifold is formed by ε-layer of instable slow motions in the neighborhood of unstable slow manifold and it is rather difficult to definitely classify the excitation. The main regime of neuron dynamics is the excitable regime, which appears in the system when ε values are small. To overcome these disadvantages the system is studied in the region which have three equilibrium states and the threshold manifold is formed by the separatrices of the saddle state (see further). The other way is to develop modified systems on its basis. Generally, the changes take place in g function in the equation for slow ion currents. For example, the model with nonlinear renewal, being a piecewise linear function, was theoretically and experimentally studied in [22, 23].

$$\begin{cases} \dot{u} = u - u^3/3 - v + I_{ext}, \\ \dot{v} = \varepsilon(\alpha u H(-u) + \beta u H(u) - v - a), \end{cases} \tag{11}$$

Where H is the Heaviside function, parameters α, β ($\alpha > 0$, $\beta > 0$) and a describe nonlinear characteristics of ion channels. On the one hand, such g function describes dynamics of ion currents in a proper way making it similar to dynamics of currents in the Morris–Lecar system. On the other hand, such modification leads to the formation of new dynamic properties of the system. In particular, studies show that compared to the classical model this system has a wider variety of dynamic regimes.

The system (11) can have either one or three rough states of equilibrium depending on the parameters. In the first case it can be both stable and unstable focus (a node). In this parameter region the system behaves in the same way as the above mentioned classical FitzHugh–Nagumo system. In the second case the phase plane has two equilibrium states of the focus (or node) type, which can be both stable and unstable, and the saddle equilibrium state. Fig. 6 presents partition of the system's (11) parameter $(\varepsilon, I_0 \equiv a + I_{ext})$ plane for three different ratios of parameters α and β in the region, corresponding to its different dynamic regimes. Phase portraits of the regimes existing in the 1–15 regions respectively are shown in Fig. 7. Phase portraits in the regions with dashes are mirror-like equivalents of the corresponding portraits without dashes. The curves A_1^+ and $A_3^+(A_3^-)$ in the diagrams correspond to the Andronov–Hopf bifurcations (change of stability) of equilibrium states O_1 and O_3 localized in the left ($u < 0$) and the right ($u > 0$) semiplanes (see Fig. 7). The superscript at A_1 and A_3 shows the sign of the first Lyapunov value. The curves H_1^+ and $H_2^+(H_2^-)$ correspond to the bifurcations of "small" loops of

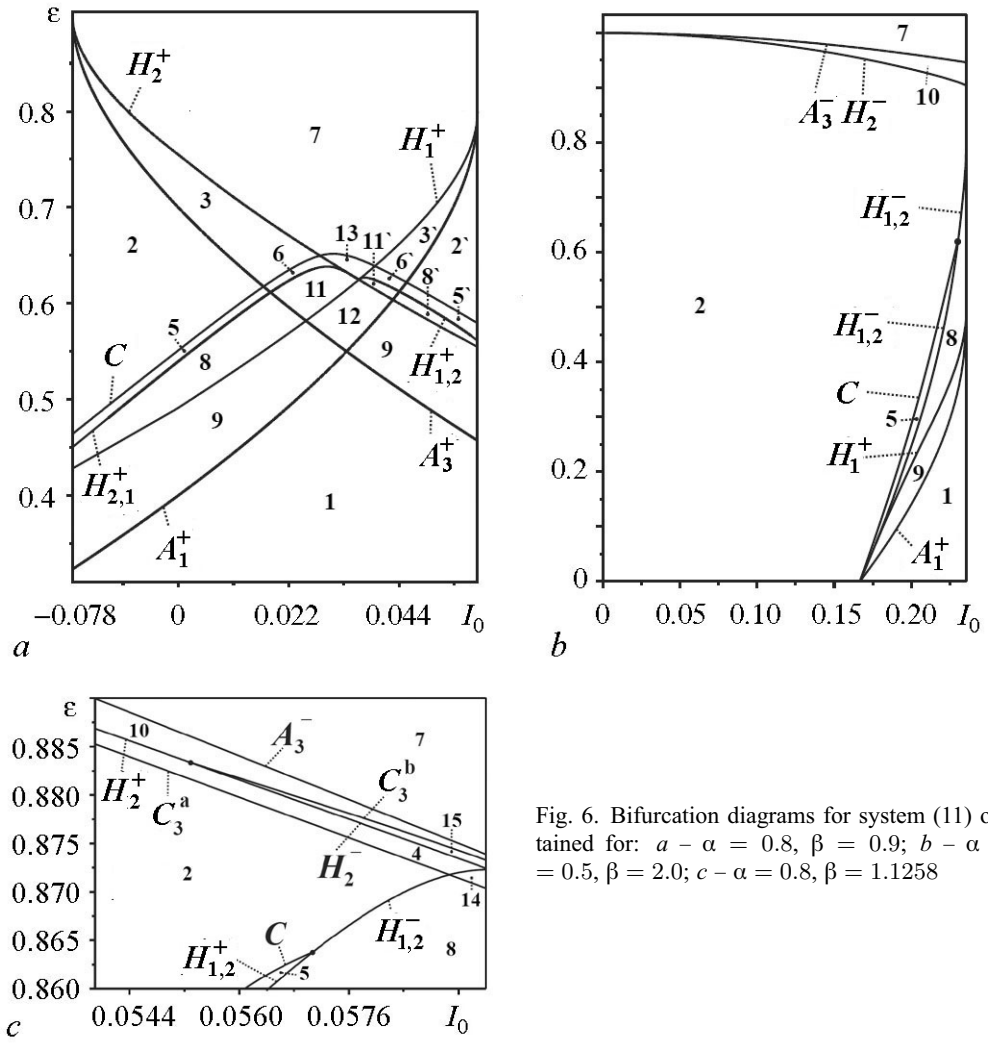

Fig. 6. Bifurcation diagrams for system (11) obtained for: a – $\alpha = 0.8$, $\beta = 0.9$; b – $\alpha = 0.5$, $\beta = 2.0$; c – $\alpha = 0.8$, $\beta = 1.1258$

the separatrices of the saddle-node equilibrium state. $W_1^s - W_1^u$ and $W_2^s - W_2^u$, and the curves $H_{1,2}^+(H_{1,2}^-)$ and $H_{2,1}^+$ correspond to the bifurcations of "big" loops of the separatrices $W_1^s - W_2^u$ and $W_2^s - W_1^u$. The superscript at H_1, H_2, $H_{1,2}$ and $H_{2,1}$ shows the sign of the saddle value. The curve C corresponds to the bifurcation of formation of the "big" double limit cycle which comprises all the three equilibrium states of the system (11) and the curves C_3^a and C_3^b correspond to the bifurcation of formation of the "small" double limit cycles, localized in the neighborhood of the equilibrium state O_3. Let us note that partition in Fig. 6, *a* can be obtained for the classical FitzHugh–Nagumo system [24], while partition in Fig. 6, *b, c* can be obtained only for models of the Morris–Lecar type.

Depending on the parameters the system can have up to three different attractors. There is one attractor in each of the regions 1 and 2 (monostability), there are two attractors in the regions 3–5, 7–10 (bistability) and the rest of the regions have three attractors (multistability). Attractors are steady equilibrium states O_1 and O_2 corresponding to the resting states and "permanent" neuron excitation respectively, the global steady limit cycle – L^s including all the three equilibrium states and corresponding to the regime of the periodic generation of excitation pulses; and local stable limit cycles l_1^s and l_1^{s*}

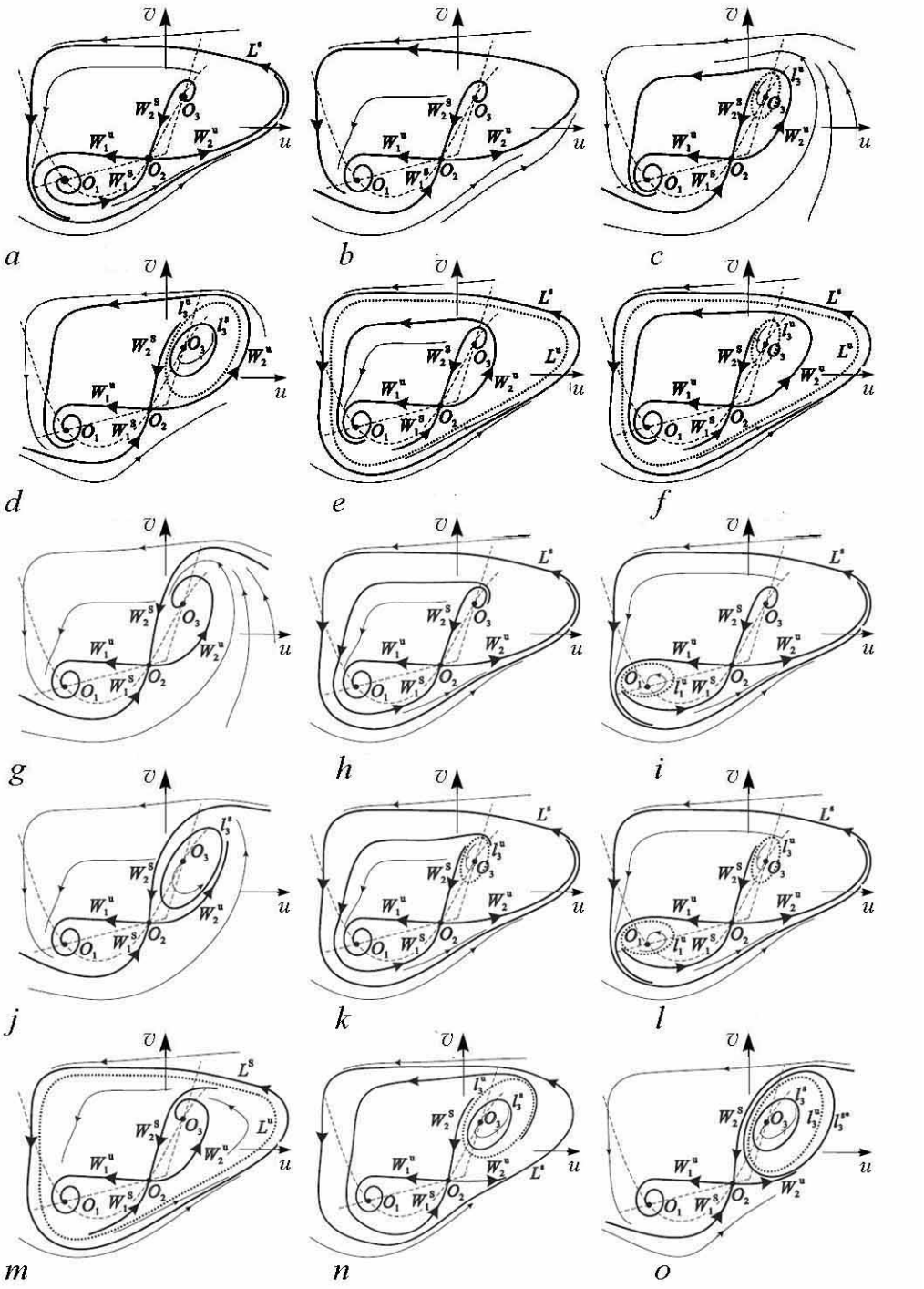

Fig. 7. Structurally stable phase portraits of system (11) corresponding to regimes in regions 1–15 (see fig. 6), respectively

(l_3^s and l_3^{s*}), including the equilibrium state O_1 (O_3) and corresponding to the regimes of subthreshold oscillations (permanent non-stationary excitation). The attractors' basins of attraction are limited to both/either stable saddle separatrices O_2 and/or global unstable limit cycle L^u, and/or local unstable limit cycles l_1^u and l_3^u including the equilibrium states O_1 and O_3 respectively. The presence of these or those attractors, threshold manifolds and their definite configurations indicate the presence of the particular behavior in the system. If the phase plane has stable limit cycles, the periodic behavior takes place. If both unstable saddle separatrices approach to one and the same equilibrium state, the excitable behavior in relation to this state takes place. If the unstable separatrices approach to different attractors or the phase plane has unstable limit cycles we encounter trigger (switching) behavior. Depending on the initial conditions in the system one attractor comes into effect. This attractor can change subsequently with the help of the external stimulus which transfers the system to the necessary attractor's basin of attraction.

Note, that all the above mentioned types of behavior can be observed simultaneously. The periodic behavior is observed in region 1. The excitable behavior is observed in regions 2–6. Besides, one can encounter transition to the permanent excitation in regions 3 and 6, and different oscillatory regimes in regions 3–6. Finally, we can observe trigger behavior between the resting state and permanent excitation (regions 7, 11–13) and different oscillatory regimes (regions 8–15).

One of the above mentioned fundamental features even for complex regimes is the presence of not more than two excitation thresholds which separate different dynamic system behavior (oscillations, resting, excitability) one from another. Let us consider the set of the system regimes (11) which have nontrivial complex-threshold dynamic properties, namely, a considerable number of excitation thresholds.

Fig. 8, *a* shows the phase portrait of one of such regimes which takes place in region 1 when the system parameters are close to the bifurcation curve, corresponding to the "big" loop of separatrix with the negative saddle value $H_{1,2}^-$ or to the curve of the "big" double limit cycle C (Fig. 6). The incoming separatrix of the saddle W_1^s approaches to the outgoing separatrix W_1^u and begins to revolve (when $t \to -\infty$) around all the three equilibrium states. On the phase plane (u, v) this corresponds to the appearance of "layerings" limited by separatrix loops W_1^s. The number of such "layerings" grows when the parameters are close to the denoted bifurcation curves and turns to infinity when the parameters match with bifurcation values. When the initial conditions agree with one of the "layerings", the trajectory, returning to the equilibrium state O_1, will make a few revolutions which means generation of the number of excitation pulses. Fig. 8, *b* shows regions p_i which determine the range of initial disturbances u_p (with u being a variable and v fixed) depending on ε-parameter. The disturbances correspond to the generation of the number of pulses $i = \overline{0.7}$. Region p_0 determines the absence of the response and region p_i determines the response in the form of a number of consecutive pulses i. It should be noted that pulse generation in this regime is possible not only for excitatory ($u_p > 0$) but for inhibitory ($u_p < 0$) stimuli. Fig. 8, *c* and *d* show system response to excitatory and inhibitory stimuli as 2 and 6 pulses respectively. Such regime can appear when the system has only one equilibrium state. For example, it can be observed when the system parameters are close to bifurcation values responsible for the appearance of the double limit cycle in its phase space. Formation of "layerings" is connected with phase trajectories accumulation. These trajectories are the result of the system dynamic memory about the recent double limit cycle.

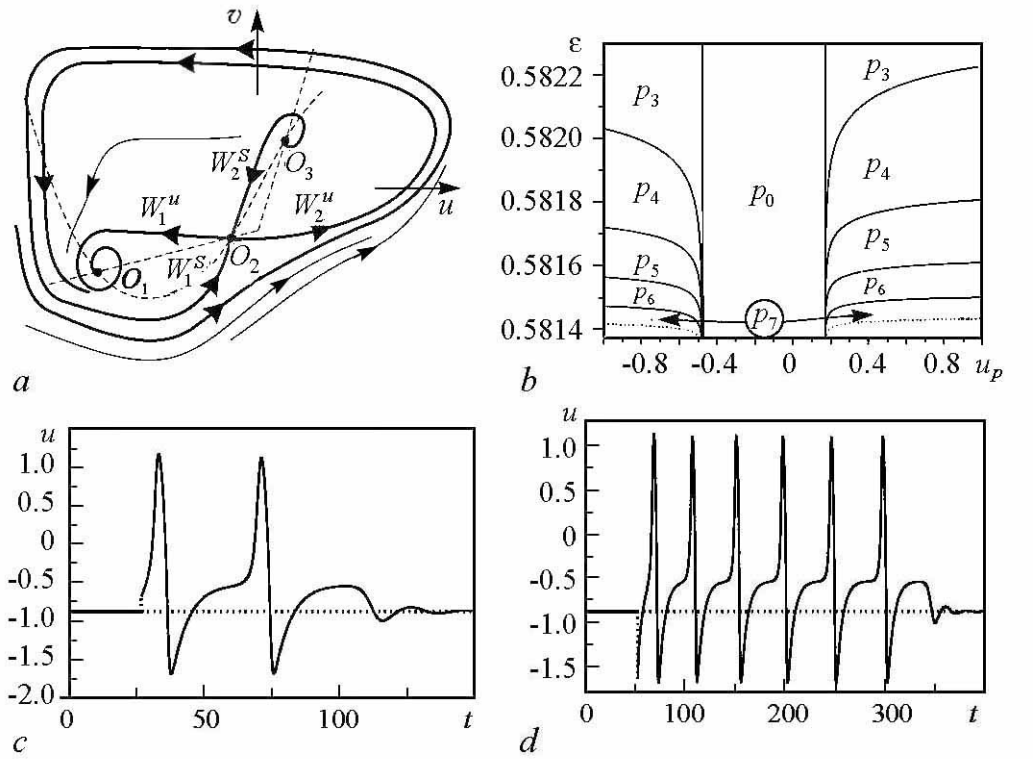

Fig. 8. *a* – excitable multi-threshold regime. *b* – areas of generation (p_i) of different number of response pulses (spike trains) depending on the amplitude of external stimulus and the parameter ε. *c–d* – the examples of responses to excitatory and inhibitory stimula. The parameters are $\alpha = 0.8, \beta = 0.9, I_0 = 0.01$

Another multi-threshold regime takes place in region 7 in the neighborhood of the bifurcation curve of the "big' double limit cycle C (Fig. 6, *a*). The typical phase portrait of this regime is shown in Fig. 9, *a*. Both incoming separatrices of the saddle begin to revolve as in the previous case when the parameters are close to C. As a result, the trigger bistable regime (transition between the equilibrium states) takes on the excitable multi-threshold properties. On the one hand, there is a possibility of pulse generation and a number of excitation pulses relative to both lower and upper equilibrium states. On the other hand, revolution of stable (incoming) separatrices leads to the appearance of nontrivial trigger behavior where transitions between equilibrium states are also followed by the generation of the number of excitation pulses. Fig. 9, *b* shows the regions corresponding to the different system behavior (11) which appears in response to resting state perturbation O_1. The regions s_i correspond to the trigger system behavior (11) followed by the generation of i excitation pulses. Figures 9, *c*, *d* show typical behavior (11) in this regime.

One more multi-threshold regime also takes place in region 10 in the neighborhood of the bifurcation curve of the "big" separatrix loop with the negative saddle value (Fig. 6, *c*). The typical phase portrait of this regime is shown in Fig. 10, *a*. Unlike the situation in the previous case, here both incoming saddle separatrices and begin to revolve around all the equilibrium states. This leads to the fact that previously simple regime with trigger-like dynamics (transitions between the resting state and local oscillations) acquires excitable-oscillatory multi-threshold behavior. Let the system (11) be in the resting state

initially. Then we can get generation of excitation pulses depending on the initial perturbation. In the end the generation will either return to the resting state or change into the regime of low-amplitude oscillations. Similar processes take place during perturbation of the system's oscillatory state.

Fig. 10, *b* shows the regions corresponding to different response of the system (11) to the perturbation of its resting system. As it was earlier region p_i corresponds to the system response in the form of i excitation pulses which return to the resting state. Region c_i also corresponds to the generation of the number of i pulses but with the following switch to the oscillatory regime. Fig. 10, *c* and *d* show both of the analyzed types of behavior.

System (11) has the same multi-threshold properties for the parameters localized near the curve C in region 8 and for the parameters localized near the curve $H^{-}_{1,2}$ in regions 13 and 15. Phase portraits of these regimes are shown in Fig. 11. These regimes have common features with the above analyzed regimes with multi-threshold properties but we will not describe them in detail.

All in all the FitzHugh–Nagumo model, which is a simple dynamic system on the plane, describe basic features of neuron dynamics in a proper way. This model comprises the presence of resting potential, the possibility of the generation of action potential, excitation threshold, refracterity etc. Dynamic regions observed in this system include excitability and periodic generation of action pulses. However, dynamics of the FitzHugh–Nagumo model can be studied with the help of qualitative methods and shown on the phase

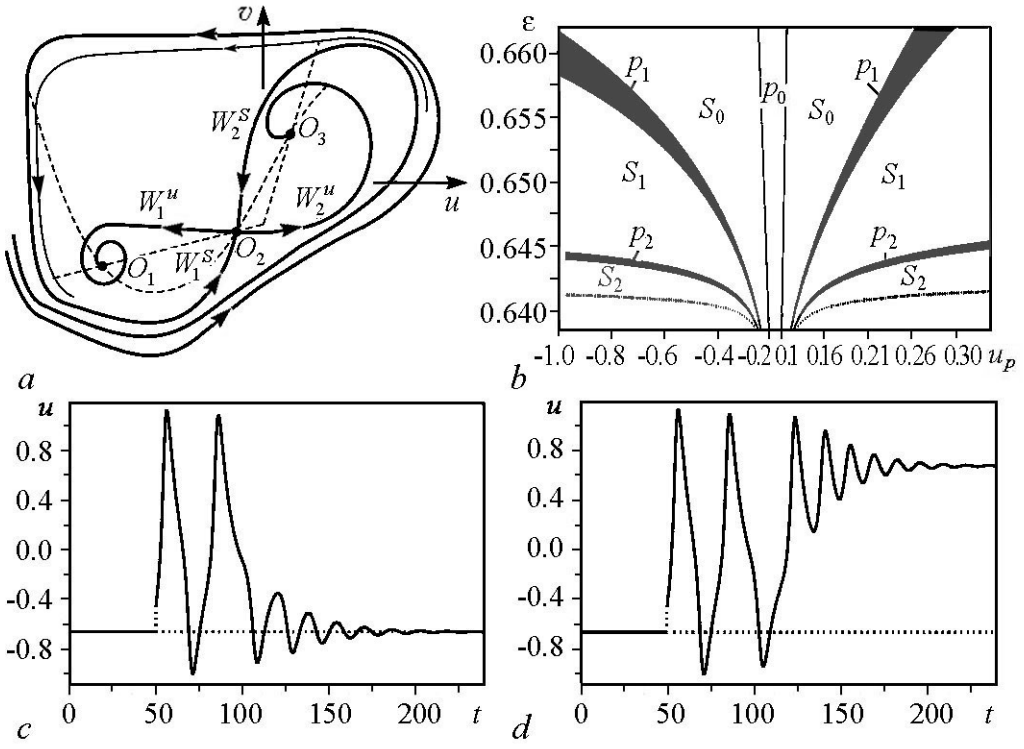

Fig. 9. *a* – excitable-trigger multi-threshold regime. *b* – areas of generation of different number of response pulses (spike trains) with either return to previous equilibrium state (p_i) or transition to another one (s_i). *c–d* – the examples of responses. The parameters are $\alpha = 0.8, \beta = 0.9, I_0 = 0.035$

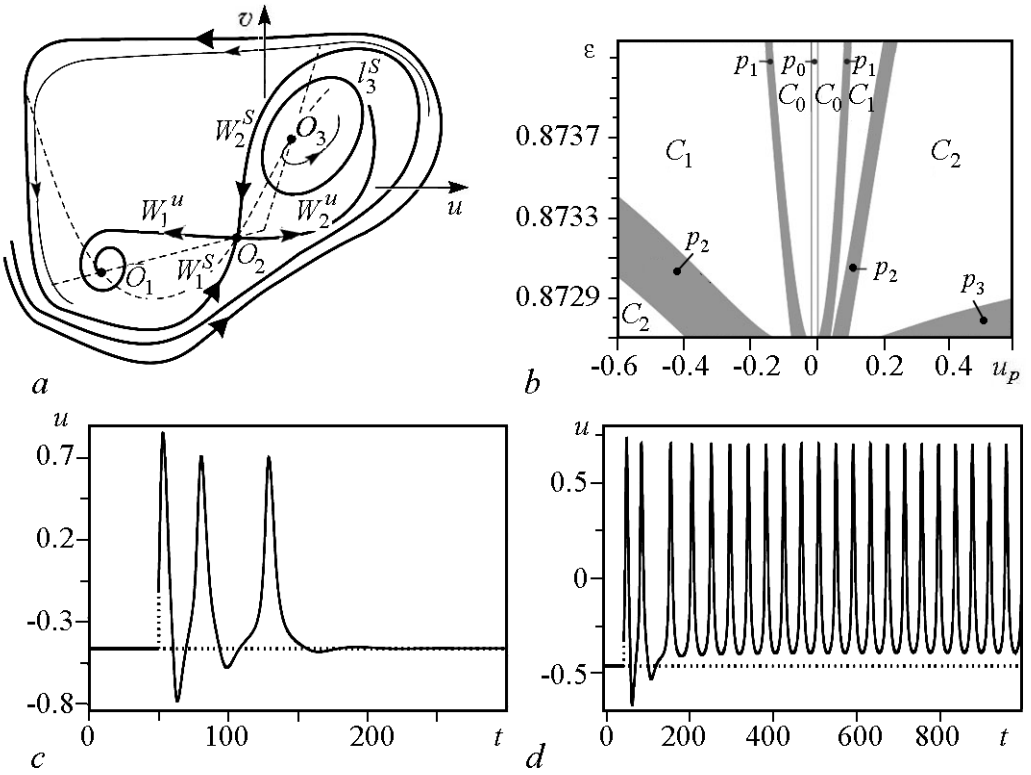

Fig. 10. *a* – excitable-oscillatory multi-threshold regime. *b* – areas of generation of different number of response pulses (spike trains) with either return to previous equilibrium state (p_i) or transition to regime of periodic spiking (c_i). *c–d* – the examples of responses. The parameters are $\alpha = 0.8, \beta = 1.1258, I_0 = 0.0595$

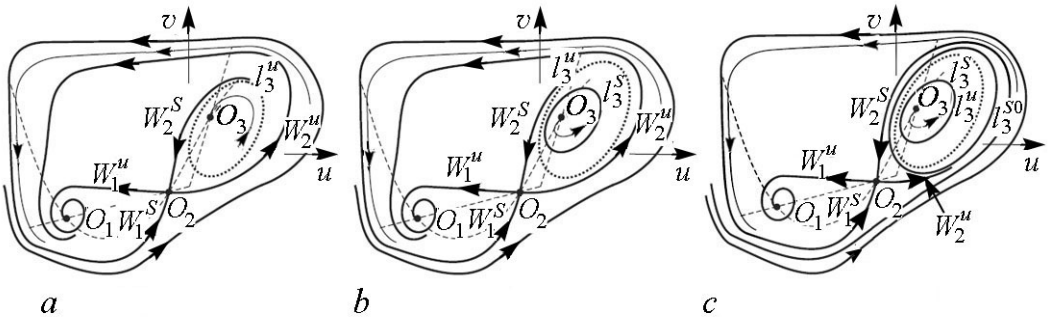

Fig. 11. *a*, *b* – excitable multi-threshold regimes with background equilibrium state (O_3) and limit cycle (l_3^s), respectively. *c* – excitable-oscillatory multi-threshold regimes with background limit cycle (l_3^s)

plane unlike the Hodgkin–Huxley model which is more complex for analytic treatment. Besides, the major feature of the FitzHugh–Nagumo models is a fairly simple way of radio technical imlemetation [16, 23, 24]. Due to the simplicity on the one hand and proper presenting of neuron basic features on the other the FitzHugh–Nagumo model is very popular with researchers.

2.4. The Hindmarsh–Rose Model. The above mentioned models of neural activity describe the neuron generation of single pulses (action potentials or spikes). However, neurophysiology has another important form of neural activity which is burst generation. Bursts present a group of two or more spikes, following each other and having periods of inactivity between them. Neural bursting was firstly suggested in the paper by Hindmarsh and Rose [25]. On the one hand, this model can be treated as generalization of the FitzHugh–Nagumo model and simplification of the physiologically realistic Hodgkin – Huxley model, on the other hand. This model is optimal in relation to the simplicity balance and the variety of dynamic regimes it demonstrates. The Hindmarsh–Rose model presents the following 3D dynamic system:

$$\frac{dx}{dt} = y - ax^3 + bx^2 + I_{ext} - z, \tag{12}$$

$$\frac{dy}{dt} = c - dx^2 - y, \tag{13}$$

$$\frac{dz}{dt} = r\left(s\left(x - x_1\right) - z\right). \tag{14}$$

Variable x describes neuron membrane potential, y and z correspond to fast and slow ion currents which flow through the membrane. Parameter $r \ll 1$ denotes the ratio of specific time scales of changes of these currents. Parameter I_{ext} describes the external current applied to neuron and other parameters characterize nonlinearity of membrane conductance. Typical values are $a = c = 1$, $b = 3$, $d = 5$ and other parameters are control ones which help to operate dynamic regimes on the system.

Due to the smallness of parameter r we can point out slow and fast motions in the Hindmarsh–Rose model [26]. The first two equations for x and y variables show fast subsystem whereas z presents a slow one. When $r = 0$ the value of variable z is fixed and becomes a parameter in the fast subsystem. The presence of two different attractors (stable limit cycle and stable equilibrium state) is the most important feature of the fast subsystem (12–13). The limit cycle corresponds to the neuron periodic generation of spikes and the equilibrium state corresponds to neuron's rest. When z increases the limit cycle disappears through bifurcation of the loop of saddle separatrices. When z decreases the state of equilibrium disappears through saddle-node bifurcation. The presence of bistability interval is the most important feature of the fast subsystem. This means that stable limit cycle and stable equilibrium state co-exist. (Fig. 12, *a*).

Slow change of variable z takes place when $0 < r \ll 1$. The attractors of the fast motions form two manifolds of in the phase space of the complete system: the equilibrium state in the fast motions corresponds to one-dimensional manifold W_0 while the limit cycle corresponds to two-dimensional manifold, which presents oscillatory surface (Fig. 12, *b*).

Stable manifolds of slow motions of the system are separated by unstable manifold W_U corresponding to the saddle of the fast motions. The boundary of the manifold W_1 is

determined by homoclinic bifurcation in the fast subsystem whereas the boundary of the manifold W_0 is determined by saddle-node bifurcation in the fast subsystem.

According to Eq. (14) dynamics of slow variable z depends on the state of the fast subsystem: if the fast motions is in the oscillatory regime, i.e. on manifold W_1, variable z increases. On the contrary, if the fast motions is in the resting state, i.e. on manifold W_0, slow variable z decreases. This means that repetitive motion on manifolds appears in the full system. At first, the representative point moves along the manifold W_1 until the edge thus increasing z. Then the system moves to manifold W_0 until the edge thus decreasing. After that the process repeats. When the representative point of the full system is close to manifold W_0, that corresponds to the hyperpolarized state of neuron, i.e. off time. When the representative point of the full system revolves around W_1, that corresponds to the generation of spikes. So, repetitive changes of manifolds correspond to the generation of a number of spikes or bursts (Fig. 13) by the full system.

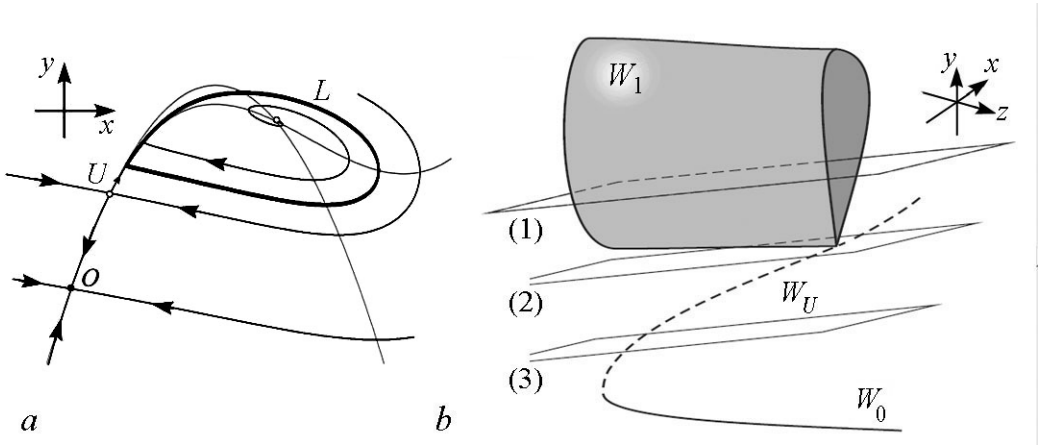

Fig. 12. a – a typical phase portrait of the fast subsystem (12)–(13) of the Hindmarsh–Rose model. The system is bistable in a wide range of parameters with a stable steady state O and a stable limit cycle L separated by a saddle U. b – a qualitative view of the full phase space of the Hindmarsh–Rose model. The stable manifolds W_0 and W_1 are separated by the unstable manifold W_U. Also depicted are three different positions of the nulcline plane for Eq. (14)

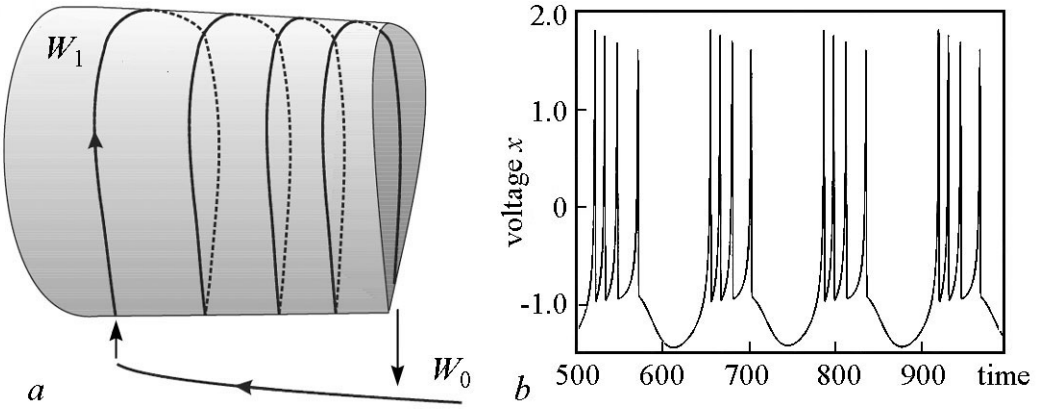

Fig. 13. Typical dynamics of the Hindmarsh–Rose system. a – sequential transitions between the manifolds W_0 and W_1. b – the membrane potential x versus time – periodic generation of burst consisting of fours spikes

Note that the speed of the system along manifolds of slow motions is determined by the plane position $z = s(x - x_1)$, which in its turn determine the nullcline of the Eq. (14). The position of this plane is controlled by parameters s and x_1, which determine the duration of bursts and off times between them. Values x_1 being large, when the nullcline plane crosses manifold W_1, the system does not leave this manifold (position (1) in Fig. 12, *b*). In this case the off time does not take place and the system generates periodic spikes with high frequency. Values x_1 being small, when the nullcline plane crosses saddle manifold, repetitive manifolds take place (position (3) in Fig. 12, *b*). The lower the nullcline plane is, the more time the system is in manifold W_0 and the longer the off time is between bursts.

The intermediate position of the nullcline plane when crossing of nullcline and manifold W_1 occurs close to the saddle (position (2) in Fig. 12, *b*) is of great interest. In this parameter region the transition from generation of spikes to burst generation takes place and this transition is the subject of research [27 29]. It should be noted that the division of system motions into fast and slow ones becomes incorrect in this parameter region. In fact, the period of the limit cycle in the fast subsystem increases greatly while approaching to the bifurcation point. Research shows that with x_1 decreasing the limit cycle corresponding to periodic spiking undergoes the cascade of bifurcations of period doubling. Strange attractor appears in the system. It is located close to the edge of manifold W_1 and corresponds to chaotic generation of spikes. The transition from chaotic generation spikes to chaotic burst generation occurs via homoclinic bifurcation in the full system. Further decreasing of x_1 leads to duration and number decreasing of spikes in bursts. Thus, transparency windows with regular burst generation appear.

As a result, the Hindmarsh–Rose model can demonstrate a wide range of dynamic regimes depending on controlling parameters. Regular and chaotic generation of spikes and bursts, and excitatory regimes refer to such regimes.

2.5. The Neuron Model with Afterdepolarization. As noted above, excitability, i.e. the ability to generate electrical pulse in response to the external stimulus of the proper amplitude, is the most important property of neuron cells. The threshold of neuron excitation is the qualitative characteristics of excitability, i.e. minimal value of the external stimulus amplitude which leads to system excitation. It turns out that the excitation threshold of some neurons is not a constant value but changes with time: the generation of one action potential may lead to temporary change of excitation threshold of subsequent pulses. This phenomenon is called afterhyperpolarization,(AHP) in case threshold rises and afterdepolarization (ADP) when threshold falls (see [30, 32]).

Afterdepolarization property of neuron membrane can play an important role in dynamics of single electrons and neuron ensembles. The falling of excitation threshold after single generation of action potential can lead to appearance of spontaneous secondary spikes or transition of neuron into the regime of burst activity. Afterdepolarization is supposed to play an important role in cognitive processes of the central nervous system, in forming the temporary memory, in particular [33, 35]. Ionic mechanisms forming the basis of afterdepolarization are not fully studied. However, the most probable mechanism is connected with a certain ion current, which becomes active shortly after neuron excitation and then gets inactivated slowly [36, 37].

The model which describes afterdepolarization property is given in paper [38]. This system is the generalization of the classical FitzHugh–Nagumo model with additional

ion current z. This current switches on quickly after the start of neuron excitation and decreases slowly after the excitation finishes. The model can be presented as;

$$\varepsilon \frac{dx}{dt} = z + I_{ext} - y - f(x), \tag{15}$$

$$\frac{dy}{dt} = a + g(x) - by, \tag{16}$$

$$\frac{dz}{dt} = \alpha(x)(1 - z) - \beta(x)z. \tag{17}$$

Here x is the membrane potential; I_{ext} is the external current, y and z correspond to two different types of ion currents, and the small parameter $\varepsilon \ll 1$ corresponds to membrane capacity, $f(x)$ is the nonlinear function having cubic form, $g(x)$ is the steadily increasing function, functions $\alpha(x)$ and $\beta(x)$ are step functions and describe activation and inactivation of the incoming ion current z.

We can identify fast and slow motions in system (15)–(17). The manifold of slow motions of the system is shown in Fig. (14). It is two-dimensional and consists of one unstable and two stable components. Stable component W_0 is located in the region of the negative x and corresponds to the unexcited neuron state, component W_1 is located in the region of the positive x corresponding to excitation.

Similar to the classical FitzHugh–Nagumo model system (15)–(17) is excitable: under the influence of a rather strong pulse the representative point leaves manifold W_0 for W_1 and neuron generates spike. After that the representative point returns to manifold W_0 and moves along it. It is important that during the motion the trajectory gets close to the edge of this manifold. When the trajectory does not reach the edge neuron returns to the resting state (Fig. 14, *a*). But the important thing is that, while the trajectory is close to the edge, membrane potential x deviates positively compared with the equilibrium state. This means that the membrane has the lower excitability threshold, i.e. the stimulus of smaller amplitude is enough for the repetitive excitation. That is the property of afterdepolarization. Dynamic mechanism, which is the basis of this property, means approaching of the corresponding to the action potential trajectory to the edge manifold which determines the threshold of system excitation.

In case the trajectory crosses the edge of manifold W_0, the neuron generates spike once more as shown in Fig. 14, *b*. This process can be repeated several times and result in periodic neuron excitation. The appearance of the regime of periodic generation of action potentials is connected with bifurcation of the double limit cycle. As a result of

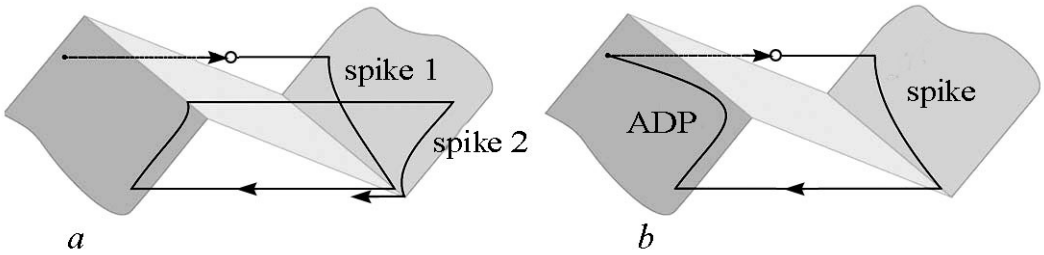

Fig. 14. Transitions between the slow motion manifolds: *a* – a single spike; *b* – tonic spiking. Modified from Klinshov V.V., Nekorkin V.I. *Communications in Nonlinear Science and Numerical Simulation*, 2012, 17(3), pp. 1438–1446

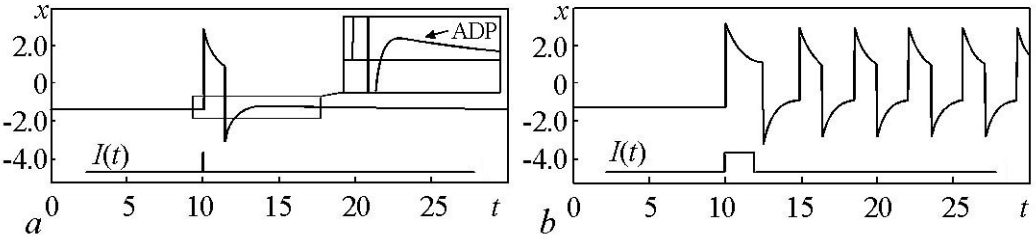

Fig. 15. The response of a neuron on external stimuli, parameters $\varepsilon = 10^{-2}$, $b = 0.5$, $\delta_0 = 0.1$, $\delta_1 = 1$, $a = -1$ are fixed, parameter γ is varied: *a* – excitability and afterdepolarization, $\gamma = 1.6$; *b* – tonic spiking, $\gamma = 2$. Modified from Klinshov V.V., Nekorkin V.I. *Communications in Nonlinear Science and Numerical Simulation*, 2012, 17(3), pp. 1438–1446

this bifurcation the stable limit cycle appears and the system becomes bistable. External stimulus leads to "switching" of the neuron from the resting state to the regime of periodic generation of action potentials (Fig. 15, *b*). Such behavior can be interpreted as dynamic memory: neuron "remembers" external stimulus and stores the information in the form of periodic activity [33].

Note, that we can observe the so called spontaneous second spikes [39, 40] near the bifurcation point in the system. Under the influence of the external stimulus the representative point gets into the region of accumulation of trajectories and makes a few revolutions and returns to the equilibrium state. This corresponds to generation of some additional spikes after the stimulation is over.

2.6. The Model of Inferior Olives Neuron. Inferior olives are one of the fundamental elements of control system and motion coordination [41] in many vertebrates especially in birds and mammals. The inferior olives convert the signals coming from cerebral cortex and spinal cord in a specific way and transmit these signals to different parts of cerebellum. The signals coming from inferior olives contain information about the plan to move. Using this information cerebellum optimizes muscle control and provides rationality, efficiency and elegance of movements.

Individual dynamics of inferior olives neurons is characterized by rhythmic oscillatory activity. This activity can be both in the form quasiperiodic subthreshold oscillations and regular generation of action potentials (spikes) [42, 43]. Besides, inferior olives neurons can also demonstrate chaotic dynamics.

Electrophysiological properties of inferior olives neurons are determined by ion currents flowing through cell membrane [44]. These currents are formed by calcium, potassium and sodium ions and possess different activation levels and operation times. Calcium ion currents take part mostly in slow processes of cell membrane depolarization and hyperpolarization, and are responsible for the generation of low-frequency subthreshold oscillations of the membrane potential. Sodium ion currents are responsible for the formation of short action potentials which, as a rule, appear on the wave of the gradual depolarization and/or in response to the excitatory stimulus. However, spike response can also appear after inhibitory stimulus (so called postinhibitory response). Potassium ion currents in inferior olives neurons play a secondary role contributing to both fast and slow dynamics.

The model described in [45, 46] is one of the simplest models of inferior olives neurons which shows qualitative correspondence with the results of natural experiments.

This model consists of two coupled subsystems. The first subsystem simulates oscillations caused by sodium ion currents while the second one simulates dynamics of calcium ion currents. The full model presents the system of four nonlinear differential equations of the first order.

$$\begin{cases} \varepsilon_{Na}\dfrac{du}{dt} = f(u) - v, \\ \dfrac{dv}{dt} = u - \big(z - I_{Ca}\big) - I_{Na}, \end{cases} \qquad (18)$$

$$\begin{cases} \dfrac{dz}{d(kt)} = f(z) - w, \\ \dfrac{dw}{d(kt)} = \varepsilon_{Ca}\big(z - I_{Ca} - I_{ext}(t)\big), \end{cases}$$

where z and w correspond to the generation of subthreshold oscillations and low-threshold (Ca^{2+}-dependent) spikes, u and v correspond to the generation of high-threshold (Na^{2+}-dependent) spikes. Parameters ε_{Ca} and ε_{Na} control time scale of the model self-oscillation. I_{Ca} and I_{Na} control the level of membrane depolarization of two subsystems, f is a cubic nonlinear function, $f(x)=x(x-a)(1-x)$. Parameter k determines the ratio of time scales of model subsystems. Value $I_{ext}(t)$ simulates the influence of external currents on neuron.

Note that the connection between calcium and sodium subsystems in (18) is unilateral. In other words the change of the value of calcium ion currents causes the change of sodium ones but not vice versa. Such configuration is called “master-slave configuration”. Thus, the oscillations of calcium ion currents in model (18) set the pace according to which dynamics of sodium ion currents is formed.

Being with appropriately chosen parameters, model (18) can generate stable subthreshold or spiking oscillations. Having chosen value I_{Ca} as control parameter we consider the oscillation mechanism in detail. Let value I_{Ca} be rather small, $I_{ext}(t) = 0$ and the system be in the resting state at the beginning. When I_{Ca} increases periodic oscillations appear in calcium subsystem as a result of supercritical Andronov–Hopf bifurcation. These oscillations, in turn, cause forced quasiperiodic oscillations in the subsystem for sodium ion currents. Such behavior is responsible for the appearance of stable subthreshold oscillations of the membrane potential in the model of inferior olives neuron.The results of the numerical simulation show qualitative matching with the data obtained *in vitro* during natural experiments (see Fig. 16) which were carried out through layer by layer examination of the guinea pig brain stem. The results were firstly published by Llinas & Yarom [47].

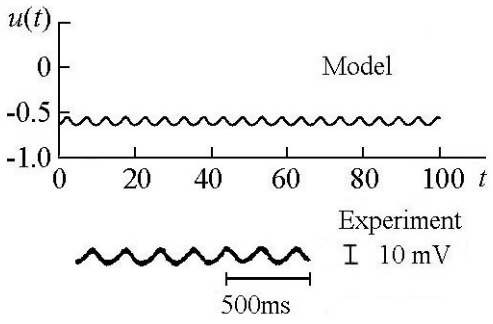

Fig. 16. Comparison of simulation results with experimental data obtained *in vitro*. Parameter values: $\varepsilon_{Na} = 0.001$, $\varepsilon_{Ca} = 0.02$, $I_{Na} = -0.6$, $I_{Ca} = 0.01$, $a = 0.01$, $k = 10$. Modified from [47]

When bifurcation parameter increases the amplitude of subthreshold oscillations in (18) grows smoothly at first,

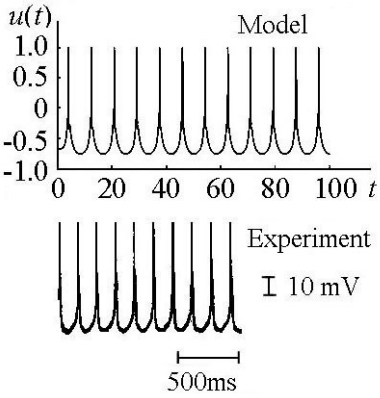

Fig. 17. Comparison of simulation results with experimental data obtained *in vitro*. Parameter values: $\varepsilon_{Na} = 0.001$, $\varepsilon_{Ca} = 0.02$, $I_{Na} = -0.59$, $I_{Ca} = 0.03$, $a = 0.01$, k=10. Modified from [47]

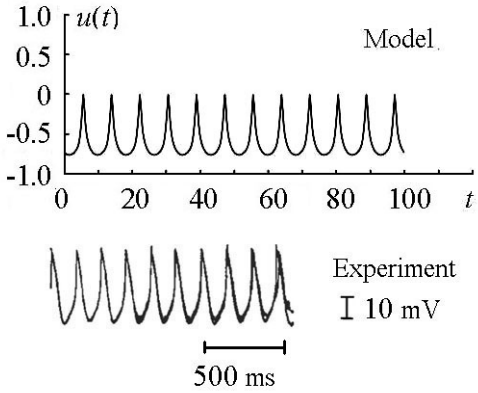

Fig. 18. Comparison of simulation results with experimental data obtained *in vitro*. Parameter values: $\varepsilon_{Na} = 0.001$, $\varepsilon_{Ca} = 0.02$, $I_{Na} = -0.6$, $I_{Ca} = 0.03$, $a = 0.01$, k=10. Modified from [47]

and the further behavior of the model depends on the value I_{Na}. If I_{Na} is rather big, the amplitude of membrane potential oscillations is higher than the excitability threshold while I_{Ca} increases in the sodium subsystem. The model begins to generate periodic relaxation oscillations of large amplitude, so called Na^{2+} or dependent spikes (Fig. 17). Note that appearance of spikes takes place on the wave of neuron membrane hyperpolarization caused by the oscillations of calcium ion currents and is determined by the phase of subthreshold oscillations. If I_{Na} is rather small, the amplitude of oscillations in calcium subsystem is not enough for the generation of Na^{2+}-dependent spikes. However, calcium subsystem possesses its own excitability threshold. When the threshold is exceeded and I_{Ca} increases the form of oscillations in the calcium subsystem is transformed nonlinearly and almost does not change with I_{Ca} further increasing. The membrane potential oscillates and these oscillations are significantly different from the quasiharmonic form of subthreshold oscillations and the amplitude is notably lower than Na^{2+}-dependent spikes. Such behavior corresponds to the generation regime of Ca^{2+}-dependent spikes observed in natural experiments (Fig. 18). Note that depending on parameters, model (18) can simulate spontaneous and forced oscillations observed in inferior olives neurons with good quality.

Model (18) is of great interest for simulation of the collective dynamics of the ensembles of inferior olives neurons. Model neurons (18) joined in the network form different structures of oscillatory activity and appear as phase-coherent clusters. Different cluster sets represent control patterns determined by the network. External signals coming to different elements can provide fast rearrangement of clusters at the network output.

2.7. The Integrate-and-Fire Model. Let us examine the neuron models of which do not need detailed description of the ion transport through the membrane.

Such models are aimed at simulation of the basic dynamic regimes and neuron properties without taking into account their physical mechanism. These models are often used for studying large neural ensembles, as they their low dimensionality helps to economize computing power. On the other hand, the simplicity of such models allows us to get analytical results for large-scale networks, e.g. by converting their dynamics to reduced equations [48–57].

The first phenomenological neuron model was suggested more than a century ago in 1907 long before discovery of the mechanisms of neuron excitability. L. Lapicque presented neuron as a shunted capacitor charged with external current. Capacitor capacitance corresponds to membrane capacitance and resistance of shunted resistor corresponds to leakage resistance. Voltages on the capacitor correspond to the membrane potential and are described with the following equation:

$$C\frac{dV_m}{dt} = I_{ext} - g(V_m - V_0), \tag{19}$$

where V_0 is the resting potential, I_{ext} is the external current applied to neuron, and g is conductance of membrane leakage. When the membrane potential reaches some threshold value $V_{th} > V_0$ neuron is considered to generate spike after which the membrane potential becomes instantaneously equal to some value $V_{reset} < V_0$.

Dynamics of such system is shown in Fig. 19, *a*. When external current is applied the membrane potential increases and when the influence is intensive enough the potential reaches the threshold value. The spike is generated then and the potential instantaneously decreases to the minimum value and increases gradually again. Due to alternation of periods of long-term potential accumulation and short-term reset such models are often called "integrate-and-fire". Accumulation corresponds to subthreshold dynamics of the membrane potential and reset corresponds to the generation of action potential.

Such models properly describe dynamics of the membrane potential lower than excitation threshold which simulates its integrating properties. From physical point of view subthreshold dynamics of this model is similar to dynamics of linear shunted capacitor (Fig. 19, *b*). Without the external stimulus the membrane potential is equal to the resting potential V_0. Non-zero external signal being at the input, the capacitor charges, however the presence of the final resistance causes leakage current. Thus, short current pulse $I_{ext} = = A\delta(t)$ leads to the exponentially decaying response $u(t) = u_0 + (A/C)\exp(-tg/C)$. As a result of the linearity of subthreshold dynamics the pulse group sent to neuron causes the response which is the linear superposition of the responses to each of the pulses. Consequently, model (19) effectively integrates input signals at characteristic time intervals $\tau \sim g/C$.

Note, that integrate-and-fire models do not describe neuron dynamics higher than the excitation threshold. When the membrane potential reaches the threshold value neuron

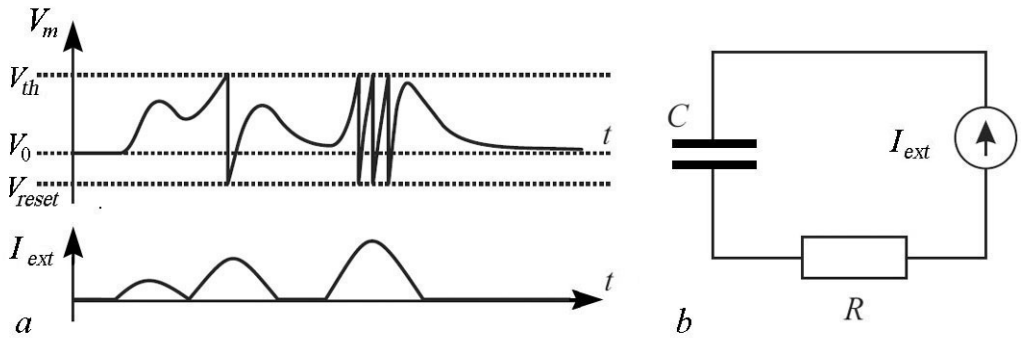

Fig. 19. *a* – dynamics of the system (19) – time dependence of the membrane potential for a given external action; spike corresponds to an instantaneous change in the value of the membrane potential from V_{th} to V_{reset}. *b* – equivalent electrical circuit

is considered to generate spike. Thus, such models do not present dynamic mechanism, form or duration of the action potential. In many cases this condition is evident because action potentials are often fixed and take place much more often than subthreshold processes. The usage of integrate-and-fire models allows us to exclude dynamics of the membrane potential during spike and simplify both computational and theoretical study.

Depending on the purpose integrate-and-fire models can have different additions for more realistic description of neuron properties. For example, to consider the property of refracterity the following detail is introduced. After spike generation the membrane potential is equal to V_{reset} for some fixed period of time τ_{ref} and neuron does not respond to external stimuli (see [59]). To take into account the properties of frequency adaptation the membrane capacitance g can be considered changing with time and described with the help of a differential equation, for example.

$$\tau_a \frac{dg}{dt} = -g,$$

where capacitance g increases instantaneously with some value Δg at every generation of spike. This modification leads to increasing of membrane capacitance when the spike is generated and to gradual decreasing of spike frequency when the external stimulus is fixed. Other methods of considering neuron adaptive properties are also possible, e.g. by adding slow ion current and considering membrane nonlinearity [60, 62].

One of the most popular is the integration-and-fire quadratic model [63–65]. In such model dynamics of the membrane potential is described with the help of the following quadratic equation:

$$\frac{dV}{dt} = I_{ext} + a(V - V_0)(V - V_{th}). \tag{20}$$

When the membrane potential reaches the value V_{th} neuron generates spike and its potential takes the value V_{reset}. Compared to the linear model the quadratic model possesses some additional properties, e.g. parameters being definite one can observe bistability between the resting regime and periodic spike generation. Model (20) is the right one for so called class one excitability connected with saddle-node bifurcation [66].

3. Discrete Models of Neural Activity

Recently new class of systems with discrete time or systems of interrelated point maps has become interesting for cooperative phenomena study in large-scale neural networks. Models in the form of point maps have a number of advantages compared with the models having the form of differential equations. For example, if we need at least two dimensions to simulate oscillatory properties in the systems of differential equations and three dimensions for chaotic behavior, in discrete time both types of dynamics can be described with only one dimension. This advantage becomes apparent in modeling complex activity regimes in single neurons and large-scale neural networks, which consist of different interacting structural units. For example, to simulate the regime of chaotic spiking-bursting oscillations (one of the most important regimes of neural activity) with the help of the systems with continuous time we will need the three-dimensional nonlinear system of differential equations. On the other hand, there are discrete models [67–69] which appear as two-dimensional point maps which simulate the regime of spiking-bursting oscillations

rather well. Point maps help simulate different regimes of neural activity. For example, the Chialvo model [70] helps simulate regimes of so called normal and supernormal excitability. The Rulkov model has some variations [71–73] one of which is adjusted to simulate different spiking and bursting oscillatory regimes while another one is capable of generating so called subthreshold oscillations, i.e. oscillations of small amplitude lower than the excitation threshold. The Curbash–Nekorkin model [74, 75] is a universal one and describes many regimes of neural activity.

3.1. The Chialvo Model. Map [70] has the following form:

$$x_{n+1} = x_n^2 e^{y_n - x_n} + I, \tag{21}$$

$$y_{n+1} = ay_n - bx_n + c. \tag{22}$$

Here variable x simulates dynamics of the membrane potential, y is the restoring variable, a, b, c and k are variables. These parameters control system dynamics in the following way: a is the restoration time constant ($a < 1$); b determines dependence of the restoration processes on the activity level: and c is constant bias. Parameter k characterizes the effect of ion currents injected in neuron. Depending on k the model dynamics can be different. The location of isoclines $y = \ln \frac{x-I}{x} + x$ and $x = \frac{-(1-a)y+c}{b}$ plays an important role in setting of this or that regime. The first nullcline is an N-curve with the maximum and the minimum, which determine threshold properties of the model. The second isocline is straight and its location defines the stability of the fixed point.

Normal excitability. In this regime the membrane potential rises monotonically to the value corresponding to the resting state. That happens after the generation of the action potential (spike) and the refracterity period. The single attractor stable node corresponds to the resting state in the model. If the amplitude is big enough to get over the threshold, the trajectory which returns to the fixed point is formed on the phase plane. This trajectory simulates the regime of normal excitability.

Supernormal excitability. The difference from the previous one is that the process of the membrane potential transition to the resting state is followed by underdamping oscillations. The fixed point stable focus corresponds to this regime on the phase plane.

Oscillatory bistability. Dynamics of the map is bistable when $I = 0.03$. Two attractors coexist simultaneously on the phase plane. They are the stable focus and the stable closed invariant curve. Their basins of attraction are separated with the unstable closed invariant curve. Depending on the initial conditions the trajectories can be attracted to one another by either the stable point or the stable invariant curve. Thus, in this case the map simulates either the regime of supernormal excitability or the regime of periodic spiking oscillations.

Chaotic spiking-bursting oscillations. It is shown that when $a = 0.89$, $b = 0.18$, $c = 0.28$, $k = 0.03$ the system has unstable fixed point and chaotic attractor in region D^+. Dynamic mechanism of chaotic oscillations means the following: as b is rather small, variable y remains in more or less "frozen" state. If we neglect the summand $-bx$ in the second equation of the system, dynamics of the variable y will be presented by one-dimensional map

$$y_{n+1} = ay_n + c \tag{23}$$

This map has a stable fixed point $y = c/(1-a) = y_0$ with a relatively big multiplier

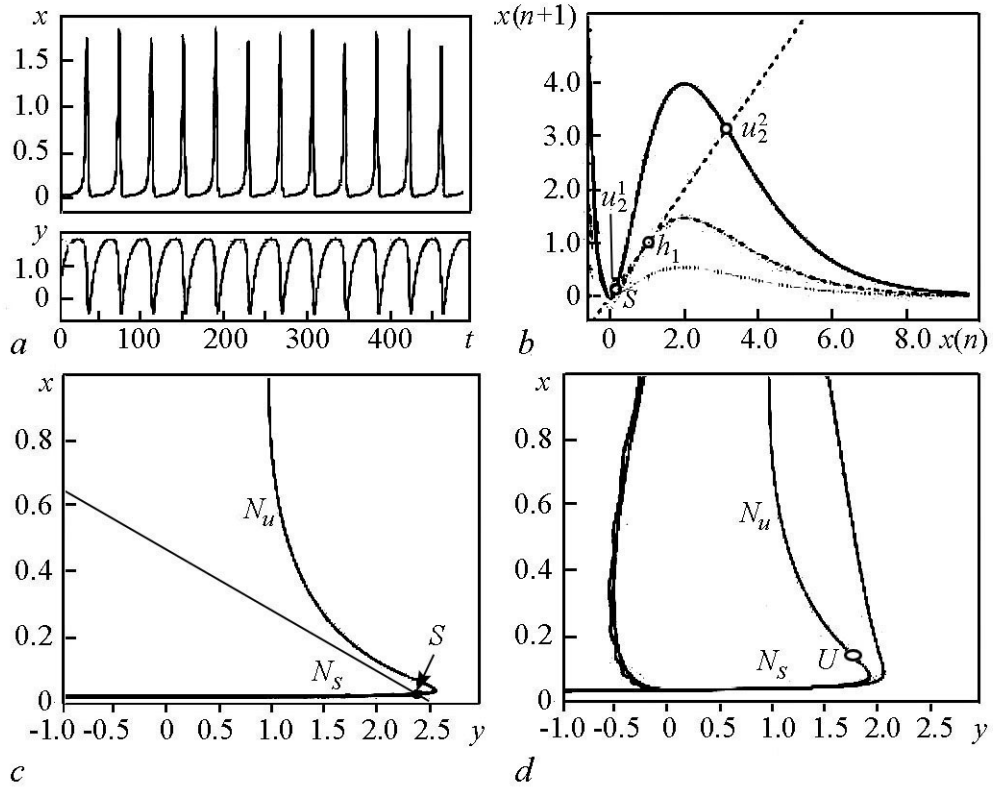

Fig. 20. *a* – waveforms for the Chialvo model in case of the spiking activity regime. *b* – the map of fast motions. *c* and *d* – phase plane with nullclines. From [68]

$s = 0.89$. That is why any trajectory mapping quickly approaches this point. In this case dynamics of the variable x is described using one-dimensional map

$$x_{n+1} = x_n^2 \exp(y_0 - x) + I. \tag{24}$$

The numeral study of this map shows its chaotic properties. Thus, relatively slow y and relatively quick x changes create the chaotic attractor in the Chialvo system. This attractor determines the regime of spiking-bursting oscillations.

3.2. The Izhikevich Model. Initially the Izhikevich model was created in continuous time but its digitalization with the time step of 1 ms gives the point map [76]

$$v_{n+1} = F\left[v_n, I - u_n\right], \tag{25}$$

$$u_{n+1} = \begin{cases} u_n + a \cdot \left[bv_n - u_n\right], & v_n < 30, \\ u_n + d, & v_n \geq 30, \end{cases} \tag{26}$$

$$F(v, I) = \begin{cases} \min(0.04v^2 + 6v + 140 + I, \quad 30), & v < 30, \\ c, \quad v \geq 30. \end{cases} \tag{27}$$

Here v is the membrane potential in millivolts and u is the slow restoration value. Parameter a is slow and separates time scales.

Parameter c determines the voltage during rearrangement. The slow subsystem has the following peculiarities: when spike is generated the slow variable becomes equal to the value of the parameter d. Fast-slow properties of the model help it simulate different types of oscillatory activity, spiking-bursting oscillations in particular (Fig. 21, *a*). Note, that the map of fast motions is the "integrate-and-fire" model. It is evident from Fig. 21, *b* where the Kñigs–Lamerey diagram for slow variable is shown. Dynamics of the full system is determined by the two-dimensional map, so the detailed information about possible dynamic scenarios is presented by nullclines on the phase plane (Fig. 21, *c*). The isocline obtained from the fast map is the parabola

$$u = 0.04v^2 + 5v + 140 + I, \quad v < 30, \tag{28}$$

which shifts to the left and to the right on the phase plane when I increases or decreases respectively. A parabola has two branches and when the value of the variable u is to the right of the parabola vertex the fast motions has two fixed points: the stable and the unstable one. Accordingly, the branches of the isocline on the phase plane (u, v) can be classified as stable (N_s) and unstable (N_u). The vertex corresponds to the point of saddle-node bifurcation of the fast motions. On the other hand, the isocline obtained from the slow motions is the inclined line. When the representative point is higher than this line the value u increases and when it is lower the value u decreases. Parameter b controls the inclination of the straight isocline. Manifolds marked in Fig. 21, *c* and *d* as M_{spikes} correspond to spike cycles of the fast motions. Their gaps determine the changes of spike periods. When the manifold M_{spikes} is higher than the slow isocline the value u increases

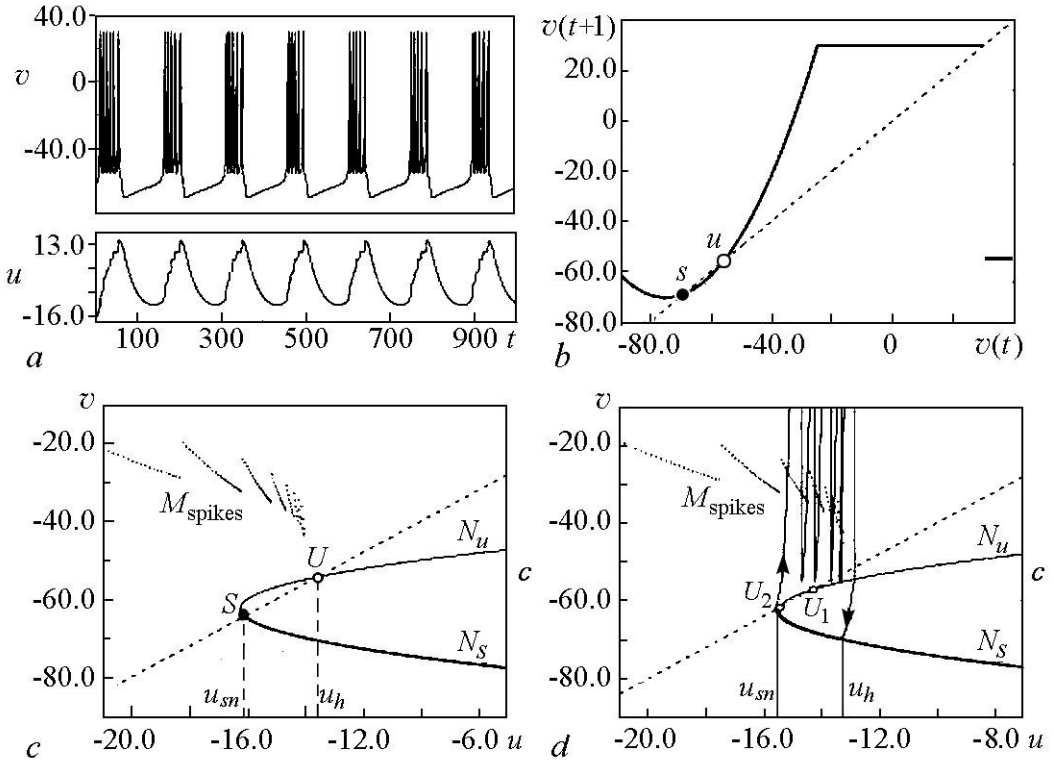

Fig. 21. *a* – waveforms for the Izhikevich model in case of the bursting activity regime. *b* – the map of fast motions. *c* and *d* – phase plane with nullclines. From [68]

along spike orbits to $u = u_h$, where the rearrangement line $v = c$ crosses N_u forming homoclinic orbit of the fast subsystem.

There can be up to two fixed points in the Izhikevich model. Their stability is controlled by the external current I and it is shown in Fig. 21, *c, d*. The difference between them consists in the horizontal shift N_s, N_u and M_{spikes}. When the value I is small enough one fixed point is stable and the other is the saddle. The neuron is in the excitable regime. Perturbation going behind the unstable branch leads to generation of the responsive action potential. When the value I increases the manifolds shift to the right and lose their stability through the Neimark–Sacker bifurcation when

$$I_{NS,Izh} = 16.25 - 62.5b + 6.25\left(b^2 - \frac{(b-a)^2}{(1-a)^2}\right).$$

This value is located around the intersection point of the slow isocline and the vertex $N_s - N_u$. It is interesting to note that S is no more a stable fixed point when the value I is a bit smaller because the Neimark–Sacker bifurcation is subcritical. After the bifurcation S becomes the unstable focus U_2. Thus the system has two unstable fixed points. The trajectory is attracted by the orbit which corresponds to spiking and bursting oscillations.

3.3. The Rulkov Model. The two-dimension map which describes dynamics of this model can be expressed as [71]

$$x_{n+1} = f(x_n, y_n), \tag{29}$$

$$y_{n+1} = y_n - \mu(x_n + 1) + \mu\sigma, \tag{30}$$

where x_n is the fast variable which shows interaction between potassium and sodium "fast" ion currents, and y_n is the slow variable which simulates the dynamic action of "slow" ion currents e. g. calcium current. Slow temporal variation of the variable y_n is motivated by the smallness of parameter μ, in most cases we shall consider $\mu = 0.001$. As shown below parameter σ sets the nonperturbed state of the model neuron. Fast one-dimensional map of the model system is made in such a way that it could be responsible for both spiking activity of the neuron and the equilibrium state. Such behavior is possible due to the special threshold function $f(x, y)$:

$$f(x,y) = \begin{cases} \alpha/(1-x) + y, & x \le 0, \\ \alpha + y, & 0 < x < \alpha + y, \\ -1, & x \ge \alpha + y. \end{cases} \tag{31}$$

Here α is the control parameter of the map. Dependence $f(x, y)$ on x obtained with the fixed value y is given in Fig. 22. The values of α and y are chosen to show the possibility of simultaneous existence of the corresponding to spiking oscillations limit cycle P_k and the fixed points x_{ps} and x_{pu}.

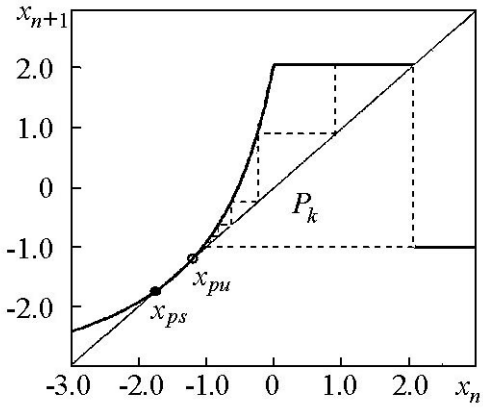

Fig. 22. Structure of the fast 1D map for the Rulkov model at $\alpha = 5.6$ and fixed $y_n = y = -3.75$. The bold solid line corresponds to $f(x, y)$. The dotted line depicts the superstable cycle P_k. The stable and unstable fixed points of the 1D map are marked by x_{ps} and x_{pu}, respectively. From [71]

The function is made in such a way that when values y increase or decrease when the dependency diagram $f(x, y)$ on x rises or falls correspondingly. The third interval is the exception. It is written as $x \geq \alpha + y$, where the values of the function $f(x, y)$ are equal to (-1).

The equation for the slow variable y_n sets the feedback and allows us to simulate both the properties of slow transitions and slow oscillations which form the pulse train of neural activity. Depending on the value of σ when α is less than 4.0 the map is either in the regime of stable equilibrium or generates continuous sequence of spikes. Thus, the frequency of pulse generation increases when the value of σ also increases. This regime is observed in the interval of the values σ which is located between the regime of continuous pulse activity and the steady-state condition. The regimes of train activity include both regular and chaotic regimes.

3.4. The Curbash–Nekorkin Model. Let us consider the system of point maps [74, 75]:

$$x_{n+1} = x_n + F(x_n) - \beta H(x_n - d) - y_n, y_{n+1} = y_n + \varepsilon(x_n - J). \tag{32}$$

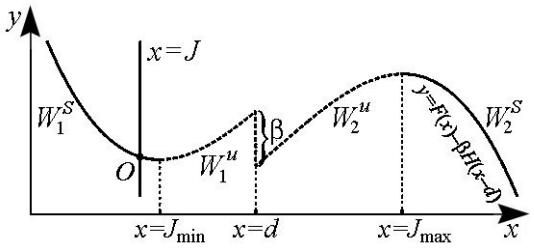

Fig. 23. Shown qualitatively are the nullclines of map (32), (33). From [77]

Here variable x characterizes qualitatively the change of the cell membrane potential; y corresponds to collective effect of ion currents (the so called restoration variable). Parameter ε determines the rate of the change of variable y, parameters β, d, J control the generated signal. Note, that the model is based on discrete variant of the FitzHugh–Nagumo system with cubic nonlinearity $F(x)$ and additionally introduced Heaviside step function $H(x)$.

$$F(x) = x(x - a)(1 - x),$$
$$H(x) = \begin{cases} 1, & x \geq 0, \\ 0, & x < 0. \end{cases} \tag{33}$$

Fig. 23 qualitatively presents the isoclines of horizontal (line $x = J$) and vertical (curve $y = F(x) - \beta H(x - d)$) inclinations of the system (32, 33) on the phase plane (x, y).

3.4.1. Regular Regimes of Activity. One of the main properties of neurons being in the resting state at first is their capability to generate the action potential when the threshold is overcome as a result of the external stimulus (the property of excitability). The stable fixed point O corresponds to the resting state of neuron in the system (32), (33). It is shown that there are two thresholds on the plane which are determined by the unstable invariant curves W_1^u and W_2^u (thin layers consisting of slow trajectories localized in the neighborhood of these invariant curves to be exact). When the system is affected by the stimulus, which is not enough to overcome the first excitation threshold (W_1^u), generation of the action potential does not take place. Only response of the small amplitude occurs (Fig. 24, *a, b* (i)). If the stimulus aplitude is enough to overcome the second threshold (W_2^u) the trajectory enters the region of attraction of the stable invariant curve W_2^s and

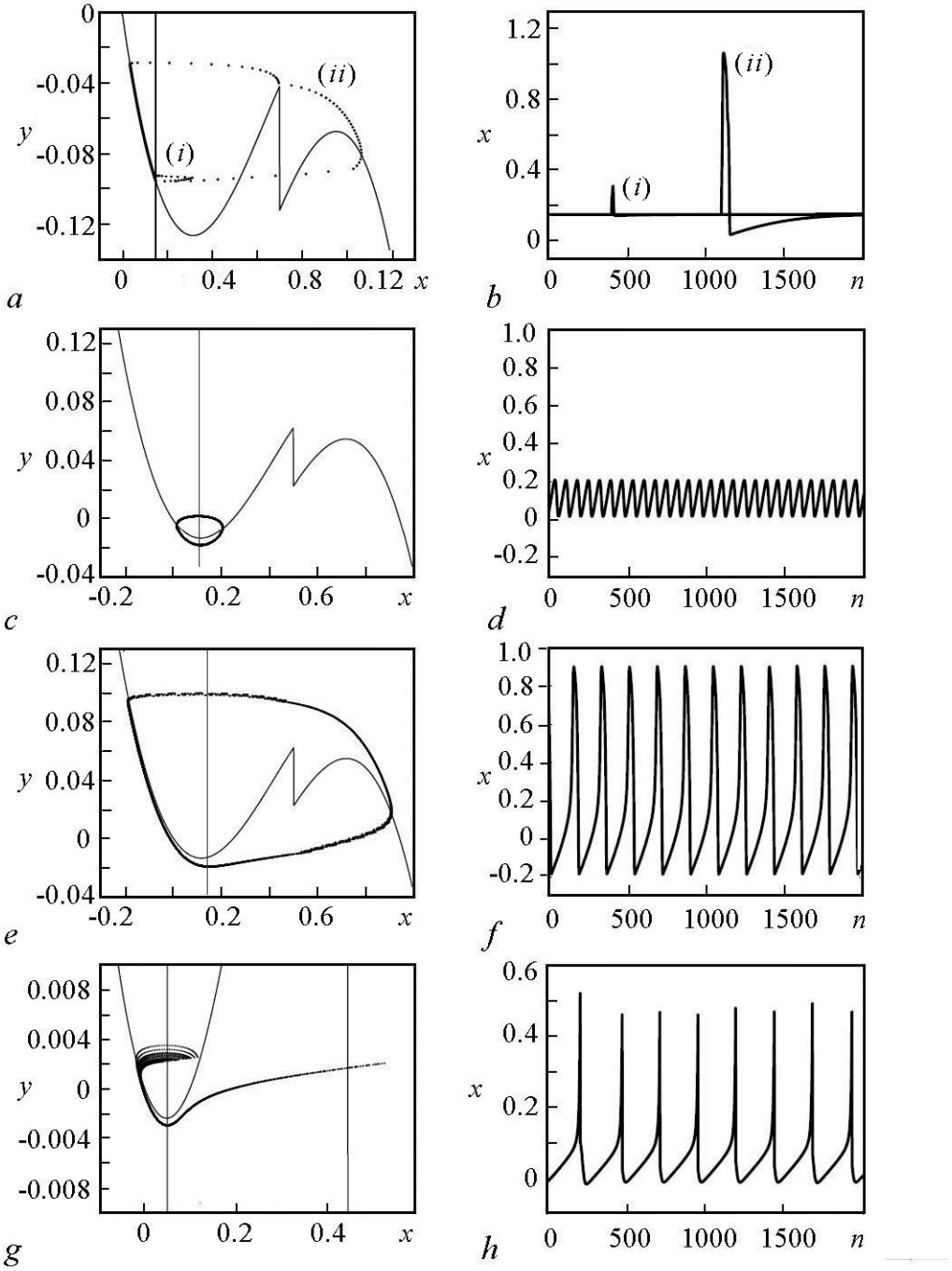

Fig. 24. Phase portraits (left column) and corresponding waveforms (right column) of regular regimes of neural activity in model (32), (33). From [77]

describes the curve which has the end in the stable fixed point O. The regime of generation of the single action potential or spike (Fig. 24, *a, b* (ii)) is the response to such behavior on the phase plane.

Subthreshold oscillations present the other important regime which is observed in the system (32, 33).The stable closed curve C (Fig. 24, *c*) corresponds to this regime on the phase plane. This curve appears when the stable fixed point changes as a result of the Neimark–Sacker bifurcation. Periodic spiking oscillations represent another steady neuron regime simulated in the system. It is found that one of the conditions of appearing of the spikes is relative smallness of β parameter. The motions between the layers of slow motions become possible. They are localized in the neighborhood of the two stable curves W_1^s and W_2^s without changing their direction when crossing the discontinuity line $x = d$. As a result the stable closed invariant curve C (Fig. 24, *e*) appears on the phase plane. This curve corresponds to the periodic spiking oscillations (Fig. 24, *f*).

Another type of spiking activity, apart from the above mentioned, is observed in model (32, 33). In such a case discontinuous attractor (Fig. 24, *g*) appears on the phase plane. This attractor determines oscillations of such form (Fig. 24, *h*).

3.4.2. The Chaotic Regimes of Activity. Different chaotic attractors can exist in systems (32, 33). One f such attractors, A, is shown in Fig. 25, *a* and the corresponding regime of neural activity is given in Fig. 25, *b*. The action potentials are generated in this regime interleaving with subthreshold oscillations. The dynamic mechanism of these oscillations is that the invariant curve W_2^u separates the system trajectories (32, 33) into two flows in the neighborhood of the discontinuity line $x = d$. The first flow forms

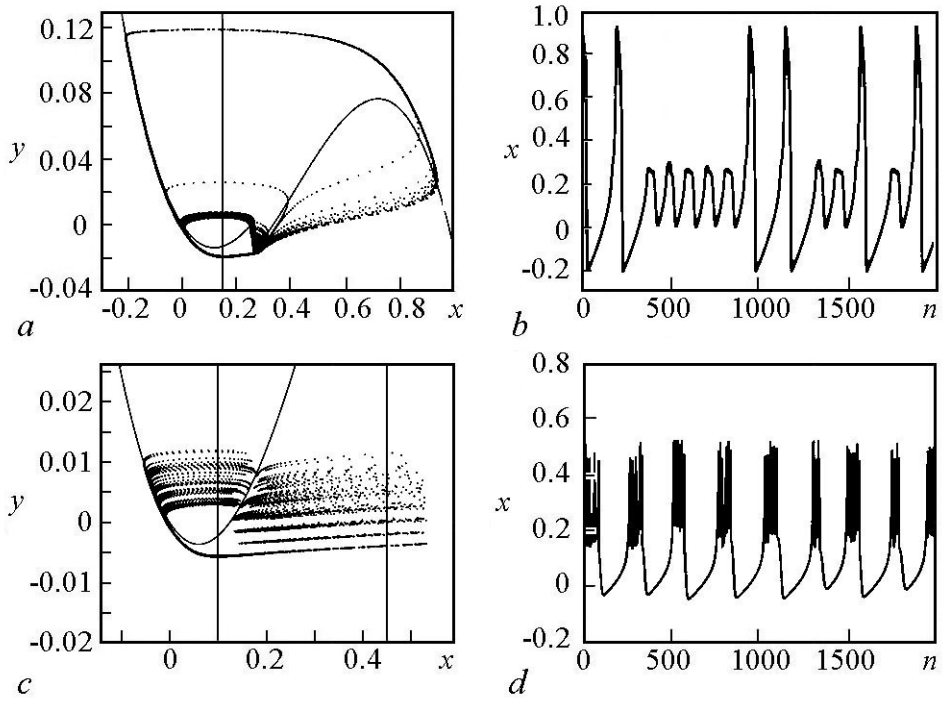

Fig. 25. Phase portraits (left column) and corresponding waveforms (right column) of chaotic regimes of neural activity in model (32), (33). From [77]

the trajectories performing the chaotic oscillations near the line $x = d$. The second flow consists of the trajectories having overcome the second threshold and moving in the neighborhood of the curve W_2^s. As a result of this separation the trajectory forms chaotically switching flow from one to other forming attractor A.

One of the most important dynamic regimes occurring in different neuron structures is chaotic spiking-bursting oscillations. In system (32, 33) this regime is simulated in a wide range of parameter values. Relaxation chaotic attractor A (Fig. 25, *c*) corresponds to this regime on the phase plane and the oscillations are shown in Fig. 25, *d*. The regime of spiking-bursting oscillations being important, we shall examine their dynamic mechanism.

3.4.3. Spiking-Bursting Oscillations. Chaotic spiking-bursting oscillations can be divided into a fast and a slow phase (see Fig. 25, *c, d*). Let us examine the formation of these two oscillations. Suppose $\varepsilon = 0$ at first and variable $y = y^0 = \text{const}$ and plays the role of the parameter in 32). Depending on value y^0 the map of fast motions (32) can demonstrate both regular and chaotic dynamics (Fig. 4). In the caseof regular dynamics the only attractor of the map (32) is the stable fixed point x_s. When parameter y^0 decreases quasistatically the equilibrium state x_s merges with the unstable fixed point at some bifurcation value and disappears (tangential or saddle-node bifurcation takes place).

In the case of chaotic dynamics the map (32) is similar to Lorenz-type map and has invariant interval which contains chaotic attractor. When parameter y^0 increases quasistatically this attractor has internal bifurcations and, finally, boundary crisis takes place (77) at some value $y^0 = y_{cr}$. One of its boundaries merges with the unstable fixed point x_u and the attractor destroys. Let $\varepsilon > 0$. In this case the group of the stable fixed points (32) forms the stable invariant curve W_1^s on the phase plane (x, y) when $x < J$. But when $x > J$, the group of one-dimensional chaotic attractors form the transient chaotic manifold. Suppose that initially the trajectory begins in the neighborhood of the curve

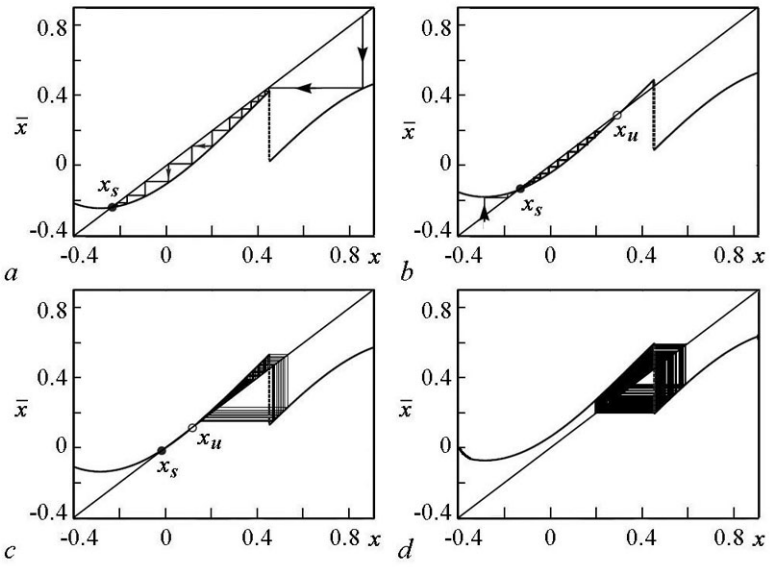

Fig. 26. Dynamics of map (32), (33) for different values of y^0: *a* – a single stable fixed point; *b* – stable and unstable fixed points; *c* – stable and unstable fixed points and an invariant interval containing a chaotic attractor; *d* – an invariant interval containing a chaotic attractor. From [77]

W_1^s. Variable y decreases slowly along this curve while variable x is maintained in the quasi equilibrium state. This phase forms the slow regular part of the two-dimensional chaotic attractor which corresponds to the passive phase of spiking-bursting oscillations.

The trajectory leaves the layer of slow motions and enters the basin of attraction of the transient chaotic manifold around the value y when the stable W_1^s and the unstable W_1^u curves merge. Being in the part of the plane where $x > J$ the variable increases slowly. Iterating the map (32) numerically we found out that chaotic oscillations persist in system (32, 33) even after the value $y^0 = y_{cr}$ which corresponds to the crisis of the chaotic attractor in the static case $\varepsilon = 0$ (Fig. 26). Therefore, the effect of disappearance delay of chaotic oscillations takes place. Such phase of motions form the fast chaotic part of attractor which corresponds to the active phase or the phase of depolarization of spiking-bursting oscillations.

Note, that the above mentioned universality of the Curbash–Nekorkin model allows us to use this model for simulating of different processes in neuron-like systems [78–91].

Conclusion

The survey presents the most popular dynamical models of neurons. Firstly, these are the models with continuous time, such as the Hodgkin–Huxley model. This model describes ion transport through neuron membrane in detail, but it is rather complicated from the mathematical point of view. The more reduced models such as the Morris–Lecar model, the FitzHugh–Nagumo model, the Hindmarsh–Rose model and the integrate-and-fire model are also presented in the survey. However they have a far lesser degree of biological relevance. Besides we describe the neuron models with peculiar properties such as afterdepolarization and bi-threshold spike generation at the background of the subthreshold oscillations. The models with discrete time, i.e. in the form of the point map, are also mentioned. Such models suggest only qualitative description of dynamics of real neurons. On the other hand, discrete models possess a variety of dynamic regimes and are suitable for numerical simulation including large-scale neural networks.

The work was done according to the state task IAP RAS (Project 0035-2014-0007 and RAS program "Nonlinear Dynamics" (0035-2-18-006) and supported by the Russian Foundation for Basic Research (grants 17-02-00874, 17-02-00904 and 18-02-00406).

References

1. McCulloch W., Pitts W. A logical calculus of the ideas immanent in nervous activity. *Bulletin of Mathematical Biophysics*, 1943, vol. 5, no. 4, p. 115.
2. Hodgkin A.L., Huxley A.F. A quantitative description of membrane current and its application to conduction and excitation in nerve. *J. Physiol.*, 1952, vol. 117, no. 4, p. 500.
3. Noble B. A modification of the Hodgkin–Huxley equations applicable to Purkinje fibre action and pacemaker potentials. *J. Physiol.*, 1962, vol. 160, no. 2, p. 317.
4. Plant R.E., Kim M. Mathematical description of a bursting pacemaker neuron by a modification of the Hodgkin-Huxley equations. *Biophys. J.*, 1976, Vol. 16, no. 3. p. 227.

5. Braun H.A., Huber M.T., Dewald M., Schäfer K., and Voigt K. Computer simulations of neuronal signal transduction: The role of nonlinear dynamics and noise. *Int. J. Bifurcation Chaos Appl. Sci. Eng.*, 1998, vol. 8, p. 881.
6. Morris C., Lecar H. Voltage oscillations in the barnacle giant muscle fiber. *Biophys. J.*, 1981, vol. 35, p. 193.
7. Keynes R.D., Rojas E., Taylor R. E., Vergara J. Calcium and potassium systems of a giant barnacle muscle fibre under membrane potential control. *J. Physiol. (Lond.)*, 1973, vol. 229, no. 2, p. 409.
8. Gutkin B.S., Ermetrout G.B. Dynamics of membrane excitability determine interspike interval variability: a link between spike generation mechanisms and cortical spike train statistics. *Neural Computation*, 1998, vol. 10, no. 5, p. 1047.
9. Rinzel J., Ermetrout G.B. Analysis of neural excitability and oscillations. Methods in Neuronal Modeling: From Ions to Networks (Eds. C. Koch, I. Segev). London: MIT Press. 1999. P. 251.
10. Ermetrout G.B., Terman D.H. Mathematical Foundations of Neuroscience. New York: Springer. 2010. 422 p.
11. Tsumoto K., Kitajima H., Yoshinaga T., Aihara K., Kawakami H. Bifurcations in Morris-Lecar neuron model. *Neurocomputing*, 2006, vol. 69, no. 4–6, p. 293.
12. Behdad R., Binczak S., Dmitrichev A.S., Nekorkin V.I., Bilbault J.M. Artificial electrical Morris–Lecar neuron. *IEEE Trans. Neural Netw. Learn. Syst.*, 2015, vol. 26, no. 9, p. 1875.
13. Abbot L.F. A network of oscillators. *J. Phys. A: Math. Gen.*, 1990, vol. 23, p. 3835.
14. FitzHugh R. Thresholds and plateaus in the Hodgkin–Huxley nerve equations. *J. Gen. Physiol.*, 1960, vol. 43, p. 867.
15. FitzHugh R. Impulses and physiological states in theoretical models of nerve membranes. *Biophysical Journal*, 1961, vol. 1, p. 445.
16. Nagumo J., Arimoto S., Yoshizawa S. An active pulse transmission line simulating nerve axon. *Proc. IRE.*, 1962, vol. 50, p. 2061.
17. Kepler T.B., Abbott L.F., Marder E. Reduction of conductance-based neuron models. *Biol. Cybern.*, 1992, vol. 66, no. 5, p. 381.
18. Andronov A.A., Vitt A.A., Khaikin S.E. Theory of Oscillators. Oxford: Pergamon Press, 1966. 815 p.
19. Mischenko E.F., Kolesov Yu.S., Kolesov A.Yu., Rozov N.Kh. Asymptotic Methods in Singularly Perturbed Systems, Monographs in Contemporary Mathematics. NY, Consultants Bureau, 1984. 294 p.
20. Arnold V.I., Afrajmovich V.S., Il'yashenko Yu.S., Shil'nikov L.P. Bifurcation theory and catastrophe theory. *Encyclopaedia of Mathematical Sciences: Dynamical Systems V.*, 1994, vol. 5, 274 p.
21. Fenichel N. Geometric singular perturbation theory for ordinary differential equation. *SIAM J. Diff. Eqns.*, 1979, Vol. 31, P. 53.
22. Nekorkin V.I., Dmitrichev A.S., Shapin D.S., Kazantsev V.B. Dynamics if a neuron model with complex-threshold excitation. *Mathematical Models and Computer Sim.*, 2005, vol. 17, no. 6, p. 75. (In Russian).

23. Binczak S., Kazantsev V.B., Nekorkin V.I., Bilbault J.M. Experimental study of bifurcations in a modified FitzHugh-Nagumo cell. *Electron. Lett.*, 2003, vol. 39, p. 13.
24. Shchapin D.S. Dynamics of two neuronlike elements with inhibitory feedback. *Journal of Communications Technology and Electronics*, 2009, vol. 54, no. 2, p. 175.
25. Hindmarsh J.L., Rose R.M. A model of neuronal bursting using three coupled first order differential equations. *Proc. of the Royal Society London B.*, 1984, vol. 221, p. 87.
26. Nekorkin V.I. Introduction to Nonlinear Oscillations. Wiley-VCH, 2015. 264 p.
27. Wang X.-J. Genesis of bursting oscillations in the Hindmarsh–Rose model and homoclinicity to a chaotic saddle. *Physica D.*, 1993, vol. 62, no. 1–4, p. 263.
28. Innocenti G., Morelli A., Genesio R., Torcini A. Dynamical phases of the Hindmarsh–Rose neuronal model: Studies of the transition from bursting to spiking chaos. *Chaos*, 2007, vol. 17, no. 4, p. 043128.
29. Shilnikov A., Kolomiets M. Methods of the qualitative theory for Hindmarsh–Rose model: A case study – A tutorial. *Int. J. of Bifurcation and Chaos*, 2008, vol. 18, no. 8, p. 2141.
30. Izhikevich E.M. Dynamical Systems in Neuroscience: The Geometry of Excitability and Bursting. Cambridge: MIT Press, 2007. 441 p.
31. Miura R.M. Analysis of excitable cell models. *Journal of Computational and Applied Mathematics*, 2002, vol. 144, no. 1–2, p. 29.
32. Yue C., Remy S., Su H., Beck H., Yaari Y. Proximal persistent Na+ channels drive spike afterdepolarizations and associated bursting in adult CA1 pyramidal cells. *J. Neurosci.*, 2005, vol. 25, no. 42, p. 9704.
33. Lisman J.E., Idiart M.A. Storage of 7 +/-2 short-term memories in oscillatory subcycles. *Science*, 1995, vol. 267, no. 5203, p. 1512.
34. Jensen O., Idiart M.A.P. and Lisman J.E. Physiologically realistic formation of autoassociative memory in networks with theta/gamma oscillations: Role of fast NMDA channels. *Learn. Mem.*, 1996, vol. 3, no. 2–3, p. 243.
35. Jensen O., Lisman J.E. Hippocampal sequence-encoding driven by a cortical multiitem working memory buffer. *Trends in Neurosciences*, 2005, vol. 28, no. 2, p. 67.
36. Haj-Dahmane S., Andrade K. Ionic mechanism of the slow afterdepolarization induced by muscarinic receptor activation in rat prefrontal cortex. *J. Neurophysiol.*, 1998, vol. 80, no. 3, p. 1197.
37. Park J.-Y., Remy S., Varela O., Cooper D.C., Chung S., Kang H.-W., Lee J.-H., Spruston N. A post-burst after depolarization is mediated by group is metabotropic glutamate receptor-dependent upregulation of Ca(v)2.3 R-type calcium channels in CA1 pyramidal neurons. *PLoS Biology*, 2010, vol. 8, no. 11, p. e1000534.
38. Klin'shov V.V., Nekorkin V.I. Model of a neuron with afterdepolarization and short-term memory. *Radiophysics and Quantum Electronics*, 2005, vol. 48, no. 3, p. 203.
39. Kepler T.B., Marder E. Spike initiation and propagation on axons with slow inward currents. *Biol. Cybern.*, 1993, vol. 68, no. 3, p. 209.
40. Enns-Ruttan J., Miura R.M. Spontaneous secondary spiking in excitable cells. *J. Theor. Biol.*, 2000, vol. 205, no. 2, p. 181.

41. Schweighofer N., Lang E.J., Kawato M. Role of the olivo-cerebellar complex in motor learning and control. *Front. Neural Circuits*, 2013, vol. 7, art. no. 94, p. 1.
42. Manor Y., Rinzel J., Segev I., Yarom Y. Low-amplitude oscillations in the inferior olive: A model based on electrical coupling of neurons with heterogeneous channel densities. *J. Neurophysiol.*, 1997, vol. 77, no. 5, p. 2736.
43. Velarde M.G., Nekorkin V.I., Kazantsev V.B., Makarenko V.I., Llinas R. Modeling inferior olive neuron dynamics. *Neural Netw.*, 2002, vol. 15, no. 1, p. 5.
44. Schweighofer N., Doya K., Kawato M. Electrophysiological properties of inferior olive neurons: A compartmental model. *J. Neurophysiol.*, 1999, vol. 82, no. 2, p. 804.
45. Kazantsev V.B., Nekorkin V.I., Makarenko V.I., Llinas R. Olivo-cerebellar cluster-based universal control system. *Proc. Natl. Acad. Sci. USA*, 2003, vol. 100, no. 22, p. 13064.
46. Kazantsev V.B., Nekorkin V.I., Makarenko V.I., Llinas R. Self-referential phase reset based on inferior olive oscillator dynamics. *Proc. Natl. Acad. Sci. USA*, 2004, vol. 101, no. 52, p. 18183.
47. Llinas R., Yarom Y. Oscillatory properties of guinea-pig inferior olivary neurones and their pharmacological modulation: An in vitro study. *J. Physiol.*, 1986, vol. 376, p. 163.
48. Klinshov V., Franovic I. Slow rate fluctuations in a network of noisy neurons with coupling delay. *EPL (Europhysics Letters)*, 2016, vol. 116, no. 4, p. 48002.
49. Klinshov V., Franovic I. Mean field dynamics of a random neural network with noise. *Physical Review E.*, 2015, vol. 92, no. 6, p. 62813.
50. Franovic I., Klinshov V. Clustering promotes switching dynamics in networks of noisy neurons. *Chaos*, 2018, vol. 28, p. 23111.
51. Brunel N. Dynamics of sparsely connected networks of excitatory and inhibitory spiking neurons. *Journal of Computational Neuroscience*, 2000, vol. 8, no. 3, p. 183.
52. Olmi S., Politi A., Torcini A. Collective chaos in pulse-coupled neural networks. *EPL (Europhysics Letters)*, 2010, vol. 92, no. 6, p. 60007.
53. Ullner E., Politi A. Self-sustained irregular activity in an ensemble of neural oscillators. *Physical Review X.*, 2016, vol. 6, no. 1, p. 1.
54. Hasegawa H. Population rate codes carried by mean, fluctuation and synchrony of neuronal firings. *Physica A: Statistical Mechanics and its Applications*, 2009, vol. 388, no. 4, p. 499.
55. Hasegawa H. Synchrony and variability induced by spatially correlated additive and multiplicative noise in the coupled Langevin model. *Physical Review E.*, 2008, vol. 78, no. 3, p. 31110.
56. Nykamp D.Q., Friedman D., Shaker S., Shinn M., Vella M., Compte A., Roxin A. Mean-field equations for neuronal networks with arbitrary degree distributions. *Physical Review E.*, 2017, vol. 95, no. 4, p. 1.
57. Montbrio E., Pazo D., Roxin A. Macroscopic description for networks of spiking neurons. *Physical Review X.*, 2015, vol. 5, no. 2, p. 1.
58. Lapicque L. Recherches quantitatives sur l'excitation electrique des nerfs traitee comme une polarization. *J. Physiol. Pathol. Generale*, 1907, 9, p. 620.

59. Lazar A.A. Time encoding with an integrate-and-fire neuron with a refractory period. *Neurocomputing*, 2004, vol. 58, p. 53.
60. Liu Y.-H., Wang X.-J. Spike-frequency adaptation of a generalized leaky integrate-and-fire model neuron. *Journal of Computational Neuroscience*, 2001, vol. 10, no. 1, p. 25.
61. Brette R., Gerstner W. Adaptive exponential integrate-and-fire model as an effective description of neuronal activity. *Journal of neurophysiology*, 2005, vol. 94, no. 5, p. 3637.
62. Abbot L.F., van Vreeswijk C. Asynchronous states in networks of pulse-coupled oscillators. *Physical Review E.*, 1993, vol. 48, p. 1483.
63. Ermentrout B. Type I membranes, phase resetting curves, and synchrony. *Neural Computation*, 1996, vol. 8, no. 5, p. 979.
64. Latham P.E., Richmond B.J., Nelson P., Nirenberg S. Intrinsic dynamics in neuronal networks. *I. Theory. J. Neurophysiology*, 2000, vol. 83, no. 2, p. 808.
65. Hansel D., Mato G. Existence and stability of persistent states in large neuronal networks. *Phys. Rev. Letters*, 2001, vol. 86, p. 4175.
66. Izhikevich E.M. Neural excitability, spiking and bursting. *International Journal of Bifurcation and Chaos*, 2000, vol. 10, no. 6, p. 1171.
67. Courbage M., Nekorkin V.I. Map based models in neurodynamics. *International Journal of Bifurcation and Chaos*, 2010, vol. 20, no. 6, p. 1631.
68. Ibarz B., Casado J.M., Sanjuán M.A.F. Map-based models in neuronal dynamics. *Physics Reports*, 2011, vol. 501, no. 1–2, p. 1.
69. Girardi-Schappo M., Tragtenberg M.H.R., Kinouchi O. A brief history of excitable map-based neurons and neural networks. *Journal of Neuroscience Methods*, 2013, vol. 220, no. 2, p. 116.
70. *Chialvo D.R.* Generic excitable dynamics on a two-dimensional map. *Chaos, Solitons & Fractals*, 1995, vol. , no. 3–4, p. 461.
71. Rulkov N.F. Modeling of spiking-bursting neural behavior using two-dimensional map. *Physical Review E.*, 2002, vol. 65, no. 4, p. 041922.
72. Shilnikov A.L., Rulkov N.F. Subthreshold oscillations in a map-based neuron model. *Physics Letters A.*, 2004, vol. 328, no. 2–3, p. 177.
73. Rulkov N.F. Regularization of synchronized chaotic bursts. *Physical Review Letters*, 2001, vol. 86, no. 1, p. 183.
74. Nekorkin V.I., Vdovin L.V. Map-based model of the neural activity. *Izvestiya VUZ. Applied Nonlinear Dynamics*, 2007, vol. 15, no. 5, p. 36. (In Russian).
75. Courbage M., Nekorkin V.I., Vdovin L.V. Chaotic oscillations in a map-based model of neural activity. *Chaos: An Interdisciplinary Journal of Nonlinear Science*, 2007, vol. 17, no. 4, p. 043109.
76. Izhikevich E.M., Hoppensteadt F. Classification of bursting mappings. *International Journal of Bifurcation and Chaos*, 2004, vol. 14, no. 11, p. 3847.
77. Maslennikov O.V., Nekorkin V.I. // Nonlinear Dynamics and Complexity (Eds. V. Afraimovich, A.C.J. Luo, X. Fu). Springer, 2014. P. 143.
78. Hess A., Yu L., Klein I., De Mazancourt M., Jebrak G., Mal H., Brugière O.,

Fournier M., Courbage M., Dauriat G. Neural mechanisms underlying breathing complexity. *PloS ONE*, 2013, vol. 8, no. 10, p. e75740.

79. Courbage M., Maslennikov O.V., Nekorkin V.I. Synchronization in time-discrete model of two electrically coupled spike-bursting neurons. *Chaos, Solitons & Fractals*, 2012, vol. 45, no. 5, p. 645.
80. Maslennikov O.V., Nekorkin V.I. Modular networks with delayed coupling: Synchronization and frequency control. *Physical Review E.*, 2014, vol. 90, no. 1, p. 012901.
81. Maslennikov O.V., Nekorkin V.I. Discrete model of the olivo-cerebellar system: structure and dynamics. *Radiophysics and Quantum Electronics*, 2012, vol. 55, no. 3, p. 198.
82. Nekorkin V.I., Maslennikov O.V. Spike-burst synchronization in an ensemble of electrically coupled discrete model neurons. *Radiophysics and Quantum Electronics*, 2011, vol. 54, no. 1, p. 56.
83. Maslennikov O.V., Nekorkin V.I., Kurths J. Basin stability for burst synchronization in small-world networks of chaotic slow-fast oscillators. *Physical Review E.*, 2015, vol. 92, no. 4, p. 042803.
84. Maslennikov O.V., Nekorkin V.I. Evolving dynamical networks with transient cluster activity. *Communications in Nonlinear Science and Numerical Simulation*, 2015, vol. 23, no. 1-3, p. 10.
85. Yu L., De Mazancourt M., Hess A., Ashadi F.R., Klein I., Mal H., Courbage M., Mangin L. Functional connectivity and information flow of the respiratory neural network in chronic obstructive pulmonary disease. *Human Brain Mapping*, 2016, vol. 37, no. 8, p. 2736.
86. Maslennikov O.V., Kasatkin D.V., Rulkov N.F., Nekorkin V.I. Emergence of antiphase bursting in two populations of randomly spiking elements. *Physical Review E.*, 2013, vol. 88, no. 4, p. 042907.
87. Maslennikov O.V., Shchapin D.S., Nekorkin V.I. Transient sequences in a hypernetwork generated by an adaptive network of spiking neurons. *Phil. Trans. R. Soc. A.*, 2017, vol. 375, no. 2096, p. 20160288.
88. Yue Y., Liu Y.-J., Song Y.-L., Chen Y., Yu L.-C. Information capacity and transmission in a Courbage–Nekorkin–Vdovin map-based neuron model. *Chinese Physics Letters*, 2017, vol. 34, no. 4, p. 048701.
89. Franović I., Maslennikov O.V., Bačić I., Nekorkin V.I. Mean-field dynamics of a population of stochastic map neurons. *Physical Review E.*, 2017, vol. 96, no. 1, p. 012226.
90. Mangin L., Courbage M. Respiratory neural network: Activity and connectivity. Advances in dynamics, patterns, cognition (Eds. Aronson, I.S., Pikovsky, A., Rulkov, N.F., Tsimring, L.S.). *Nonlinear Systems and Complexity. Springer Int.* 2017. vol. 20. p. 227.
91. Yang X., Wang M. The evolution to global burst synchronization in a modular neuronal network. *Modern Physics Letters B.*, 2016, vol. 30, no. 14, p. 1650210.